Mechanical Behaviour of Nanocrystalline Rhodium Nanopillars under Compression

by

Omar Alshehri

A thesis

presented to the University of Waterloo

in fulfillment of the

thesis requirement for the degree of

Master of Applied Science

in

Mechanical Engineering - Nanotechnology

Waterloo, Ontario, Canada, 2012

Author's Declaration

I hereby declare that I am the sole author of this thesis. This is a true copy of the thesis, including any required final revisions, as accepted by my examiners.

I understand that my thesis may be made electronically available to the public.

Abstract

Nanomechanics emerged as chemists and physicists began fabricating nanoscale objects. However, there are some materials that have neither been fabricated nor mechanical investigated at the nanoscale, such as rhodium. Rhodium is used in many applications, especially in coatings and catalysis. To contribute to the understanding the nano-properties of this important material, rhodium was fabricated and mechanically investigated at the nanoscale. The nanopillars approach was employed to study size effects on mechanical properties. Nanopillars with different diameters were fabricated using electroplating followed by uniaxial compression tests. SEM was used as a quality control technique by imaging the pillars before and after compression to assure the absence of buckling, barrelling, or any other problems. Transmission electron microscopy (TEM) and SEM were used as microstructural characterization techniques, and the energy-dispersive X-ray spectroscopy (EDX) was used as the chemical characterization technique. Due to substrate induced effects, only the plastic region of the stress-strain curves were investigated, and it was revealed that rhodium softens with decreased nanopillar diameter. This softening/weakening effect was due to the nanocrystallinity of the fabricated pillars. This effect is consistent with the literature that demonstrates the reversed size effect of nanocrystalline metals, i.e., smaller is weaker. Further studies should focus on eliminating the substrate effect that was due to the adhesion layers between Rh and the silicon substrate being softer than Rh, consequently, causing Rh to sink into the adhesion layer when compressed and thus perturbing the stress-strain curve. Moreover, further investigation of other properties of Rh is required to achieve a

comprehensive understanding of Rh at the nanoscale, and to render it suitable for specific, multivariable applications.

Acknowledgements

It is very difficult to express complete gratitude and thank everyone that helped me along with this project as there were a lot of them along the way. Among many examples, the funny emails filled with jokes that my brother Ali sent regularly helped me overcome many frustrating moments I went through during the course of this project. With that said, listing all those who helped me might double the number of pages of the thesis. Therefore, I would like to thank those who had major contributions to this project.

First and foremost, all praise and thanks are due to Allah, the Sustainer of this universe, the One without whom I would not be able to breathe let alone finishing this project with virtually no scientific background at the beginning of it.

I thank Zeinab Jahed for her continuous initiative to help me during all my lab works. Without such initiative to help, this project would have taken twice the effort that it took.

Thanks also to Prof. Mustafa Yavuz for accepting me as his student and for his constant encouragement since our first meeting. Without that acceptance I would not be in the nanotechnology field.

I wish to thank Dr. Ting Tsui for requiring me to write a weekly summary about three papers related to the project. Without such request at early stage, writing the thesis would have been frustrating.

Thanks also to Elfaitori Ibrahim who introduced to me and taught me how to use EndNote program and the “rice cooker”. EndNote saved me tens of hours of frustration

coming from typing and renumbering references, while the rice cooker saved my time and rescued my stomach, and pocket!

I have an un-payable debt to my best friend and teacher; the one who stayed with me all the times, day and night; the one who taught me many concepts in science and engineering from scratch; the one who without him, I would not be able to learn most of what I learnt: Thank you so much YouTube.

Dedication

To all those going to their laboratories driven by a sincere, true welling to know what is really happening down there at the atomic level, not by a desire to compete with other groups or to lengthen their publication list. To them I say: “I found for you some stuff going on down there.”

To all mothers who are doing the greatest job a woman has had: To stay home growing up prophets, scholars, worshippers, commanders, workers, engineers, scientists and future mothers to keep the humanity going through stable childhood, antidepressant-free youth, and peaceful elderly life!

Table of Contents

List of Figures

List of Tables

"Rushing in responding to peoples' questions is either a sign for the shallowness of knowledge or for its breadth and copiousness."

Ibn Al-Qayyim (1292-1350 CE)

1. Introduction

1.1. Photography and the Genealogy of Nanoscience[1]

Science is a collective effort; any idea or invention used nowadays is underpinned by huge human endeavour, and nanoscience is no exception. Therefore, it is worth mentioning how nanoscience evolved in order for us to have a map that leads us to how to proceed along the same path.

Overall, the advancement of physical sciences is based mostly on the advancement of photography. For example, the introduction of the first commercial video tape recorder by a research team at Ampex© led by the American engineer Charles Ginsburg in 1951 [2] excelled some branches of science and created new branches such as "motion and time study" that changed the way companies manage and engineer their manufacturing processes, and made much more money from the same amount of "motion" and time [3]. On the other hand, telescopes that were first invented in Holland in 1608 started cosmology, the way humans understand the outer space, rather than astrology, because telescopes allowed humans to "see" the shape of the space rather than guessing it. Photography all started in by Alhasan ibn Alhaytham (965 – 1038), one of the Islamic world's medieval scientists (known in English as Alhazen) who is called the "first true scientist" [4] as he was the first in history to write what is now known as a "scientific paper" when he wrote down the procedures of the experiment he did step by step to make

[1] "Nanoscience" is a name that has no physical sense to it [1]. Nano is nothing but a number. Therefore, saying nanotechnology or nanoscience is like saying fivetechnology or pointsixscience. Therefore, it is better to be linked with the unit "meter" to indicate that it is a science related to the dimensions. Consequently, it is more accurate to call it "nano*meter"* technology or "nanometer *scale"* technology. Another example is that "femtolaser" is more accurately "femto*second* laser". However, for consistency with the literature, it will be referred to as "nanoscience" or "nanotechnology".

it repeatable. Alhaytham wrote books documenting his experiments about the anatomy of human eyes, light, and many others. One of his experiments was conducted to understand optics, because Ptolemy had a theory of optics that was not logical according to Al-Haytham. Ptolemy thought of the images seen by eyes as a result from a light that is emitted from the human eyes, hitting an object, and finally return to the eyes as an image of that object [5]. This paradigm was completely changed by Al-Hasan ibn Alhaytham's books in light and sight [6, 7] especially *Kitāb al-Manādhir*[2] (The Book of Optics). Firstly, he logically falsified the contemporary idea that the eye emits light to see objects by asking about how eyes do not see at night. He concluded that the eye receives the light emitted/reflected from object and decided to study this reception process. Al-Haytham built a dark room, the first camera obscura, and made a very small hole to let the light in. Surprisingly, Al-Haytham saw the image of the surroundings outside the room but upside down. After that he wrote his procedure, his observations, and an interpretation with a suggested mechanism [6]. *Kitāb al-Manādhir* had a profound impact on the West after been translated into Latin in the early thirteenth century under the title *De aspectibus* [8].

After that scientists started to study light and its reflections, images, and the human eyes until the first optical microscope appeared in Holland in 1590 by Hans Jansen and his son Zacharias [5, 9]. The optical microscope opened and excelled many branches in science such as bacteriology, biology, and medicine [5]. After that the researchers' endeavour was towards improving the magnification ability of the optical microscopes and understanding how to utilize them to see the finer details of the materials and set the rules for the newly observed entities. This effort involved many scientists including Galileo in

[2] It is written in the literature as *al-Manāzir*, where the closest transliteration from Arabic to English is what is written above: *al-Manādhir.*

1609 and Marcelo Malbeja in 1661 both in Italy, Robert Hock in England in 1665, and Jan Swammerdam in 1670 and Van Leeu Antonie van Leeuwenhoek in 1673 both in Netherlands (Holland previously), and others.

However, another way of dealing with nature started to rival the oneness of experiments. At the end of 19th century the theoretical physics started to form itself as a distinct branch of science, because the theoretical physics' predictions of the 18th century and the beginning of 19th started to match reality with high accuracy. As a result, the widely unknown scientist back then Richard Feynman had the confidence to predict the ability of seeing and manipulating atoms, as he presented in his 1959 talk titled "There's Plenty of Room at the Bottom" [10] at the California Institute of Technology. Inspired by the talk, the scientific community launched an expedition to search for atoms until 1983 when the major breakthrough came from IBM labs when Gerd Binnig and Heinrich Rohrer invented the scanning tunnelling microscope (STM) [11] enlightened by the work of Ernst Ruska, the inventor of the first electron microscope [12]. Therefore, STM enabled scientists to see (what is seen is a drawing of the atom; atoms cannot be seen until now) the internal microstructure of matter. This opened a whole new realm of science: nanoscience. The researchers started to see the materials that they were imagining with the help of mathematics and the 2D characteristic techniques such as x-ray diffraction. Obtaining a 3D image of the materials turned the research effort from imagination and verifying imagination towards direct observation.

1.2. Further than Nanometer

Following the nanoscience revolution, another photography-based revolution came by Ahmed Zewail in 1988 when invented the Femto-Laser [13] where the very basic

interaction between atoms in the molecule became visible. Likewise, this invention created what is called femochemistry. This laser launched "The World's Fastest Camera" [14]. After about twenty two years Zewail et al. [15] invented the first "atomistic video tape recorder" which is called 4D microscope where it is possible to see the interaction between atoms in time – time being the fourth dimension. In other words, Zewail and coworkers made it possible that, instead of imaging the interactions between atoms in a certain point in time like a camera, the interactions between atoms could be seen in real time – like a video recorder. Zewail in his Nobel interview predicted that it might be possible to create an attolaser that would enable scientists to see interactions between electrons [16]. Such a laser might unravel the very promising atto-technology or "quantumtechnology."

1.3. The Mechanism of Nanoscience

Materials that we commonly deal with are called "macromaterials". Macro means large, and macromaterials are materials that can be seen by the unaided eye. However, many think that nanomaterials cannot be seen by the unaided eye which is incorrect: in some cases it can be and in others it cannot. Understanding this requires an explanation of the mechanism behind nanoscience.

Every material is composed of atoms. These atoms are not bonded like a network; instead, they group as aggregates (particles) where each aggregate has millions of atoms that will form a ball-like shape. Each aggregate is bonded to other aggregates by a force that is weaker than the force bonding two atoms. For macromaterials, the diameter of an aggregate is in the range of microns. When these aggregates (i) get separated and then (ii) each split into two smaller ones where the diameters of the two halves are in the

nanometer realm and then (iii) they re-assembled, this material becomes a visible nanomaterial. So it is basically reconstructing the materials with smaller building blocks. But when the micrometer wide aggregates split and do not re-assemble, the splitted aggregates become an invisible nanomaterial that could be used in any nanodevice. The disassembly of aggregates and the splitting process is called top-down fabrication, while the re-assembly of the split up aggregates is called bottom-up assembly.

Figure 1.1 shows both kinds of nanomaterials and the corresponding fabrication technique. In both visible and invisible nanomaterials, the properties of these nanomaterials are significantly different than the original material. For example, gold is no more "golden" in the nanoscale and the color of it is deep red [17], the graphite that is mechanically and electrically weak becomes the strongest material on earth (i.e., carbon nanotubes) [18] or a theoretical superconductor (i.e., graphene) [19]. The reason behind these changes is that as the aggregates become smaller, the number of atoms on the surface of the aggregate becomes comparable to the number of the interior atoms. As all of the chemical reactions (e.g. bonding) and most of the physical process (e.g. electricity conduction) are carried out by electrons, more surface atoms leads to more surface electrons ,leading to more reactions/processes.

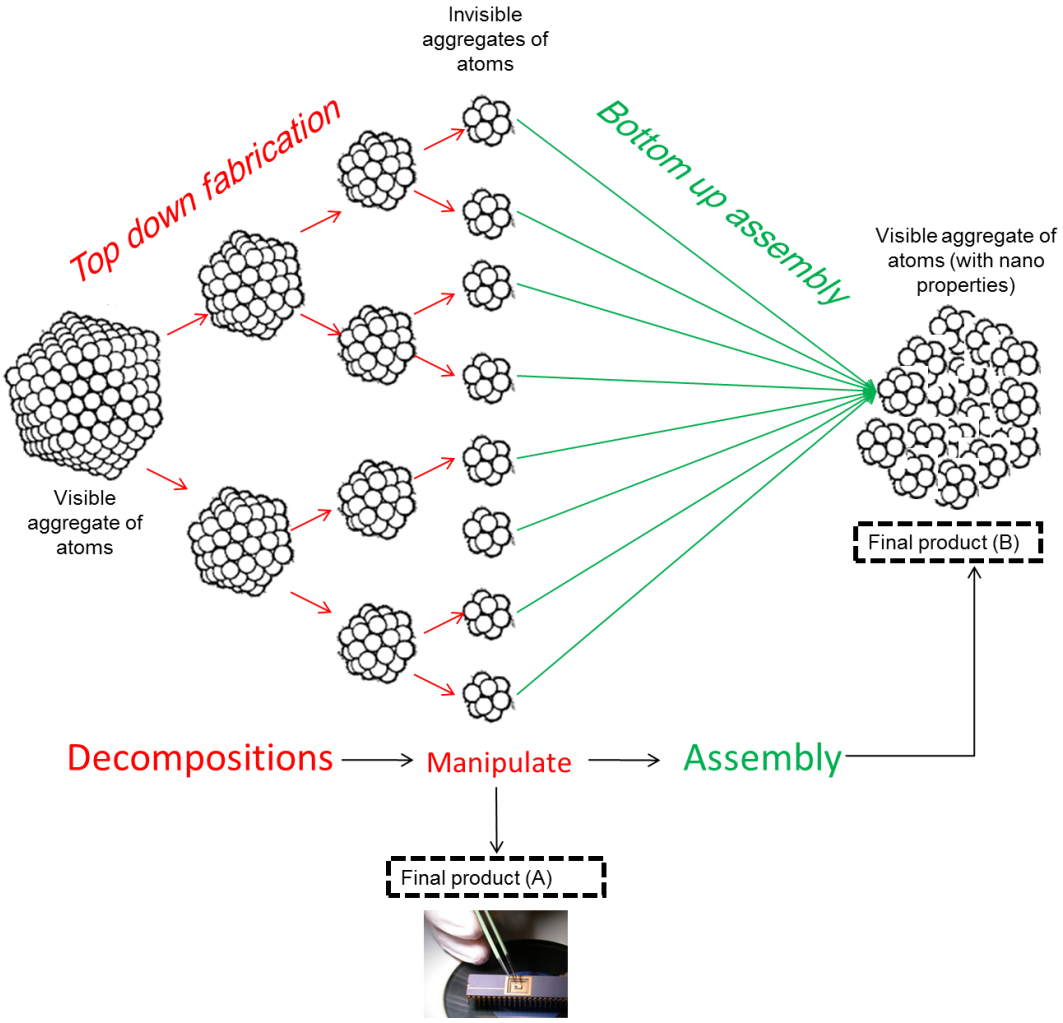

Figure 1.1: The two fabrication approaches for nanomaterials: Top-down decomposition of materials (left to middle), and bottom-up assembly of the decomposed materials (middle to right).

Ozin et al. [20] provided a very expressive and informative cartoon images - Figure 1.2 - to visualize the top-down and bottom-up fabrication approaches in nanoscience.

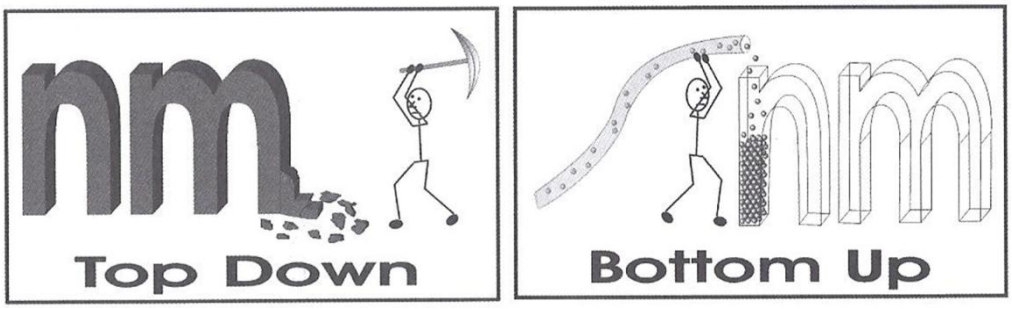

Figure 1.2: Images illustrating top-down (left) and bottom-up (right) nanofabrication approaches. Reproduced with permission from [20].

The ratio of surface atoms to total atoms is usually called “surface-to-volume ratio,” an expression that needs to be linguistically revised as any ratio should have a numerator and denominator with the same units which is not the case in the above expression because it gives a surface to volume not a surface to surface or volume to volume ratios. Therefore, it might be called surface-to-volume “factor.”

1.4. Definition and Branches of Nanoscience

Having described nanoscience, a definition and classification may be given considering the aforementioned understanding. In general, any new field should be preceded by a theoretical definitions and classification to organize the tremendous information and ideas into main streams or categories, so as to allow a comprehensive view for the field to identify areas for further inquiry and to direct efforts towards solving them. Consequently, many scientists, engineers and technologists have tried to provide a short meaningful definitions and classifications of nanoscience/technology. Before listing different definitions and classifications, it is essential to distinguish between science, engineering, and technology. Among the many definitions provided by researchers, science, engineering, and technology could be defined as follows:

Science: The study of nature as a whole and as individual entities to discover the properties and characteristics of it, without necessarily knowing the practical benefit of such discoveries.

Engineering: The use of or reconciliation between scientific discoveries to produce products that have useful, practical purpose(s).

Technology: The use of or reconciliation between engineering products to produce new products that have personal attachment with humans.

In the nano realm, the borders between science and engineering are vague as any research in the nanofield requires engineering to fabricate the material and science to study it. Therefore, Nayfeh et al. [21] stated that scientists became engineers in this field. However, nanotechnology is used to represent nano-science, engineering, and technology throughout the literature. After clarifying the differences between the three branches, nanotechnology in the coming chapters will be used to represent the three branches for writing convenience. Having read many definitions for nanotechnology, it could be defined as the following: *The study and the application of materials where the material grains have surface atoms comparable in number to the total number of atoms of grains.*

In the new definition of nanotechnology above, no upper and lower dimensional limits are provided, in contrary of all definitions in the literature. This is because there is no clear cut boundary for when the nanophenomenon ends at. For example, Rogers et al. [22] and Ozin et al. [20] defined the boundaries of nanophenomenon from 1 to 1000nm, while Barth et al. [23] set them as 0.1-100nm. The aforementioned limits certainly do not exclude the 1001 nm diameter particle from the nano-stage. Therefore, in both cases no scientific proofs were provided for establishing such sharp boundaries. The truth is that the limits of the nanoeffect are different for different materials, shapes/structures, feature sizes, and temperatures. For example, Uchich et al. [24] reported that for small scale pillars the transition from bulk to nano-behaviour occurred at a diameter of 42 μm. Therefore, for certain material (Ni_3Al-Ta), certain shape (pillar), certain feature size (diameter), and certain temperature (room temperature) the boundary upper limit was 42

μm, a dimension significantly greater than any value in the literature. Consequently, associating the "nano" to the small scale technology might need revision. However, "nano" word association might be overridden in the sense that the vast majority of phenomena are in the order of magnitude of 1-1000nm.

1.5. Mechanics of Small Scale Materials

Small scale mechanics emerged after the industrial revolution (note that *mechanics* here is meant for the solid-state material mechanics). The concern was over precise machining processes, such as lathing and milling, where parts of the machine (mostly the cutting tip) were manufactured with a micrometre precision. Therefore, these parts were extensively studied and examined mechanically. Short after, the invention of transistors and other electronic materials caused a rapid growth of the microelectronics industry that urged researchers to study these micro-sized materials. Hence, the field started to assemble as a separate branch of research where, for example, the words *thin film* and *MEMS* (Microelectromechanical systems) became part of the widely known scientific vocabularies. This continued until the invention of the STM that revolutionized small scale mechanics by pushing it further into the nanoscale. The interesting turn point is that with the nanomaterials' exceptional behaviour, the research in mechanics became a highly motivated area of research, in addition to industrial purposes, for merely scientific curiosity. Further discussion will be dedicated to nanomechanics. In general, what is applicable for nanomechanics is applicable for micromechanics, however, the results are completely different.

There are many methods used to study the mechanical properties of materials. For small scale mechanical properties, the possibility of using all these methods is low, because of

either technical or cost-related reasons. The methods that have been applied to study small scale mechanics are as follows:

1- Nanoindentation [25].
2- Uniaxial tension [26].
3- Uniaxial compression [24].
4- Three/four point bending [27].
5- Plane-strain bulge testing [28].
6- Crack propagation testing [29].

All the above methods should presumably lead to the same conclusion about certain properties. However, there are properties that cannot be studied by all of the above methods. The factors that limit the number of tests that can be applied are as follows:

- **The property that is intended to be investigated.** For example, yield point cannot be determined by nanoindentation test.
- **The physical properties of the material under testing.** For example, graphene cannot be studied by nanoindentation as there is no thickness for graphene to be penetrated.
- **The chemical properties of the material under testing.** For example, sticky materials cannot be studied by plane-strain bulge test as they will stick and contaminate the surface of the bulge.
- **Embedded inaccuracies.** For example, nanoindentation introduces a nonuniform distribution of the mechanical strains within the contact area because of the sharp

pyramid tips which “locally concentrate stress at the apex of the contact and along the edges of the pyramid” [30].

- **The shape of the specimen.** For example, spheres cannot be studied by Plane-strain bulge test.
- **The cost of the test.** For example, uniaxial tensile test for nanopillars is very costly and technically difficult, because it involves many nanofabrication techniques (for sample preparation) and the tests and their setup must be done individually for each sample which limits the number of tests that can be done.

1.5.1. Uniaxial compression of nanopillars

In general, the most common technique for exploring nanoscale mechanical properties with the least limitations and drawbacks -especially the absence of the drawback of the presence of strong strain gradients- is the uniaxial compressive loading of cylindrical nanopillars fabricated by focused ion beam (FIB) milling alone [24] or electron beam lithography coupled with electroplating [31]. This nanopillar compression approach to study the mechanical properties at small scales was first introduced in 2004 by Uchic et al. [24] for microsized pillars, and later extended to the nanoscale in 2005 by Greer et al. and others [32].

In such a test, compression is applied using a nanoindentation device outfitted with a flat tip (no nanoindentation involved; nanoindentation here is used as a tool where the tip is larger than the pillar and is neither round nor pyramidal; instead, a flat tip acting as a compression tip). The stress-strain curve is simultaneously drawn for the compressed pillar.

1.6. Rhodium and Some Selected Properties

Rhodium is a rare and expensive member of the platinum group metals [33]. It was discovered in 1803-1804 by the English chemist William Hyde Wollaston in a crude platinum ore [34]. These ores are located in Canada, Colombia, Abyssinia (Ethiopia now), former USSR countries, USA, and South Africa [35]. In its bulk form, pure solid rhodium has a silvery white color [36] and rosy solutions. Rhodium has a face-centered cubic (fcc) crystal structure with no allotropes [37] and an atomic number of 45 with an electronic configuration of [Kr] $4d^8$ $5s^1$ that has thirty-eight isotopes [38]. Practically, rhodium is more difficult to work with than other metals of similar crystallographic structure, such as Cu, Ag, Au, Pt and Pd [37]. This is partly due to its high melting temperature, 1960 °C, which makes it difficult to be heat treated, for example. Table 1.1 lists some properties of rhodium.

The property	Its value	The reference	Note
Atomic number	45	[39]	---
Atomic weight	102.91	[39]	---
Atomic diameter, *k*X	2.7	[39]	---
Measured density, kg/m^3	12.4	[39]	---
Theoretical density, kg/m^3	12.4	[39]	---
Lattice constant: a, Å	3.7957	[39]	---
Nuclear spin: *I*	½	[40]	---
Magnetic moment: μ_{Rh}	-0.088 μ_N	[40]	---
Resistivity, μΩcm	4.51	[40]	at 20 °C
Superconducting transition temperature, μK	325	[41]	---
Resonance frequency, Hz	50	[41]	at zero field
Melting temperature, °C	1960	[39]	---
Measured boiling point, °C	4500	[39]	---
Calculated boiling point, °C	4150	[39]	---

Table 1.1: Selected rhodium properties and their numerical values.

1.7. Applications of Rhodium

Bulk Rh has three main application categories: as an alloying agent, a catalyst, and a reflective coating. For the usage as an alloying agent, Rh is mainly alloyed with platinum and palladium as in the fabrication of airplane spark plugs [36]. For catalysts applications, Rh is used as a catalyst in automobile exhaust [42, 43]. Due to its high reflectivity [44], Rh is used as reflective film in solar mirrors [45].

In the nanosize -especially the nanopillars-, the applications of Rh nanopillars are falling in the general scientific and technological applications of reconstructed matter into shaped building blocks. These applications include [20] batteries, fuel cells and photovoltaic, digital imaging and printing, microelectronic packaging, controlled chemical release, chemical sensing and molecule separations, catalysis and photocatalysis, combinatorial materials chemistry, microfluidics and lab-on-chip, nanoelectronics, nanophotonics, nanomagnetics, and other ramifications in science and technology. Applying rhodium nanopillars for a specific use requires extensive studies for other nanoproperties (in addition to the current reporting of the nanomechanical properties.)

1.8. Fabrication of Rhodium Samples (Nano- and Bulk Samples)

1.8.1. Fabrication of Rhodium Nanosamples

The Rh nanopillars were fabricated by electroplating. The chips were fabricated in the Emerging Communications Technology Institute at the University of Toronto by electron beam lithography coupled with the electroplating technique. But before describing the

details of fabrication process, it is worth mentioning other Rh nanopillars fabrication methods and justify why electroplating was chosen.

There are six methods for forming Rh nanodeposits (thin films and/or nanopillars):

1- Electrospinning [46].
2- Plasma-enhanced chemical vapour deposition [47].
3- Physical vapour deposition [48-52].
4- Electrochemical deposition [53].

Among the above techniques, electrochemical deposition (i.e. electroplating) was chosen for several reasons. First, it is a high quality and low cost process. Second, it is simple relative to other techniques that require sophisticated machines and equipments. Third, electroplating provides the possibility of fabricating sub 100nm pillars [26, 54] which is difficult with other methods. Moreover, electroplating yields better filling of the templates as the reduction process occurs for each individual atom; hence, better hole or template filling.

1.8.2. The fabrication and mechanical properties of bulk Rh samples

Rhodium is one of the least studied of all metals for two reasons. First, it is extremely difficult to work with [55, 56]. It was suggested that this difficulty might be due to the presence of impurities, while another suggestion is that a transformation takes place to some other crystal structure [55]. However, Bale [55] showed that no allotropic transformation will occur if the test is carried out at a temperature below 1500 °C. The second reason is that rhodium is an expensive and rare metal. This is why Maurer et al. [57] reported in 1997 that the "experimental data concerning the elastic behaviour of pure

single-crystalline rhodium are hard to find in the literature" and they only found one paper concerning it. However, their sentence holds true in the "google era": there are only five papers that have studied the mechanical properties of non-alloyed or pure rhodium [39, 55-58] where two of them [57, 58] neither discussed the plastic properties nor used the conventional tension/compression method but rather applied the ultrasonic attenuation approach [57, 58]. The other three papers used the uniaxial tension test (no compression test was reported).

Holden et al. [39] fabricated rod-shaped Rh samples by two methods: (i) as-received annealed specimens (no information on how the as-received specimens were fabricated) and (ii) annealed electron-beam floating-zone melted specimens. Both methods produced polycrystalline Rh rods. However, the final microstructure (after the test) depended on the temperature at which the tests were carried out: the grain growth was larger for 500 and 1000 °C tests while the grains were small for the test at 750 °C. The authors did not mention the microstructures for samples that were tested at other temperatures – the temperature range was from -196 to 1000 °C.

The impurities of the as-received specimens were $\leq$ 0.09 % by weight, while for the ebeam-melted samples the impurities were 0.01911 or 0.2881 % by weight, depending on the cooling rate. The samples were annealed after that.

1.9. The Mechanical Properties of Bulk Rhodium Samples

For the aforementioned bulk samples of Holden et al. [39], the samples were tested with a displacement rate of 0.0127 cm/min with a strain rate of 0.019 cm/min. Table 1.2 summarizes the tensile test results obtained for the two fabrication methods used. The authors noticed that the transition from ductile to brittle behaviour occurred at temperatures < -196 °C.

As-received Rh rods (high purity), and annealed for ¼ hour at 900 °C.					
Temp., °C	Homologous temperature, $T(K)/T_M(K)$	Ultimate tensile strength, MPa	Proportional limit, MPa	0.2 % offset yield strength, MPa	Reduction of area, %
-196	35	862	64	92	27.8
25	134	707	49	67	22.5
250	235	610	74	95	59.4
500	347	336	58	75	32.4
750	458	117	24	40	≈90
1000	572	85	24	34	Severe surface cracking noted
Electron-beam melted, swaged 80% at 900 °C, and annealed at ¼ hour at 800 °C.					
-196	0.035	1.027	0.323	368	---
25	0.134	0.759	0.234	265	42
250	0.235	0.627	0.258	286	55
500	0.347	0.426	0.247	293	35
750	0.458	0.225	0.217	---	≈100
1000	0.572	0.089	0.022	30	35 (slight surface cracking noted)

Table 1.2: Tensile properties of bulk rhodium samples under various conditions. Reproduced with permission from [39] with stress unit converted from psi to MPa.

The very low value of 0.2 % yield stresses observed by Holden et al. [39] was observed also by Bale [55] who obtained a 0.1 % proof stress of 63.40 MPa. However, Bale suggested a mechanism to interpret such peculiarity: the tensile stress-strain curve had no elastic region; rather, the diagram showed a smooth plastic curve from the origin which meant that Rh was soft at the onset of the deformation, but experienced very rapid strain

hardening from onset of the deformation. Bale suggested that this mechanism for the deformation of Rhodium which has fcc structure -unlike any other fcc metal- might be due to slip systems other than that known for fcc metals. The samples Bale used were made of Rh powder that were pressed, sintered in oxygen-free hydrogen, cold worked, and then annealed in a high vacuum. Then the annealed specimen was formed into sheets 0.1524 millimeters thick. The specimens contained less than 10 ppm of metallic impurities.

Looking at all values above, it is clear that the most suitable and proper value of yield point to show the size effect (by comparing it to nanopillar yield points) is the value of the as-received sample at 25 °C temperature (room temperature), which is 67 MPa. This is because the other samples are swaged, which mean the samples are tubular. Therefore, the as received samples with the rod-shape were tested at the same temperature as that of the nanopillars (room temperature), which make it the best fit for the purpose of this study. The manifestation of size effect upon scaling from bulk to the nanoscale will be discussed in the coming chapter.

2. Experimental

Intelligent use of data requires an understanding of how the data are obtained [59], and this will be mentioned below. Therefore, the following figure depicts the several steps that transformed the raw material into nanopillars and how they were investigated.

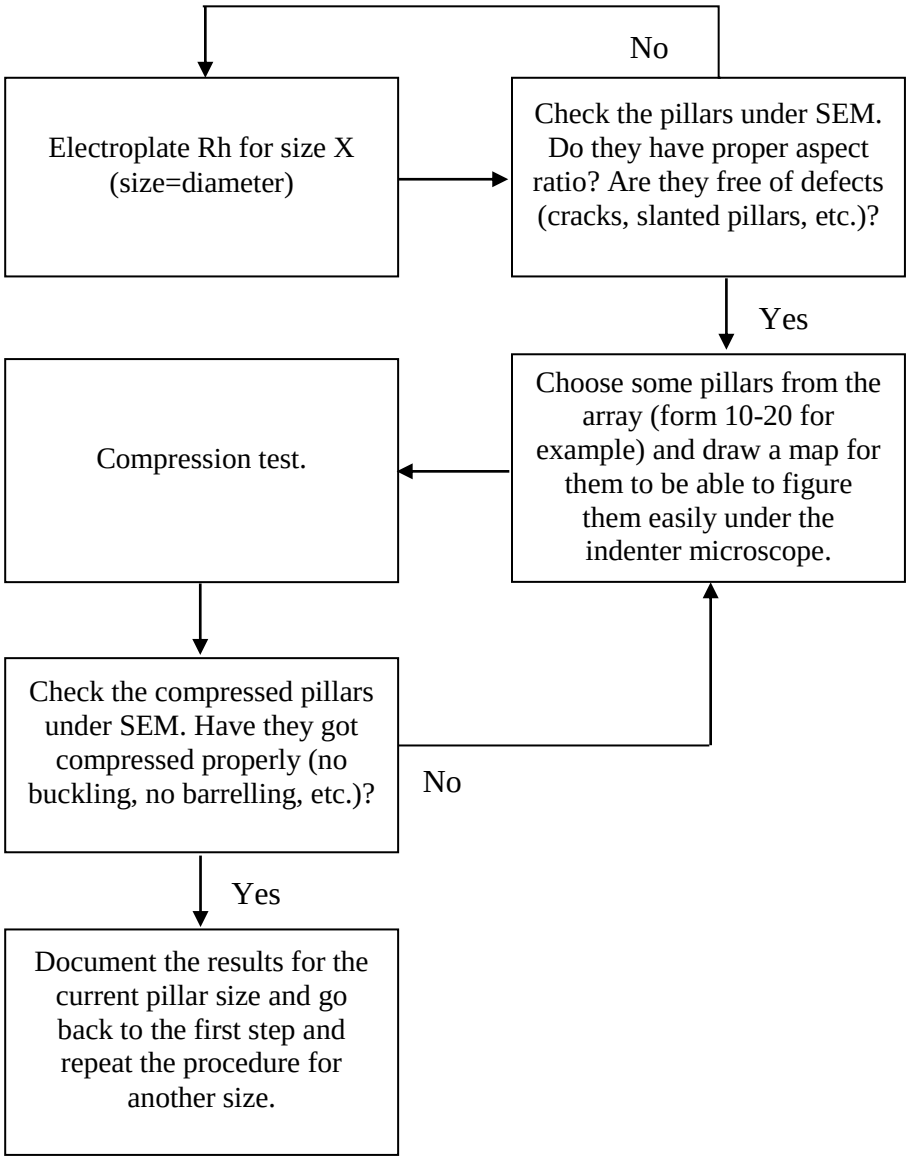

Figure 2.1: The different steps that are used to study the mechanical properties of Rh nanopillars.

2.1. Electrodeposition (electroplating) of Rh nanopillars

Electroplating was done on custom made chips. The fabrication of these chips is described in detail in [31, 60]. In brief, the chip is formed from four materials: silicon, titanium, gold, and poly(methylmethacrolate) (PMMA) as shown in Figure 2.2.

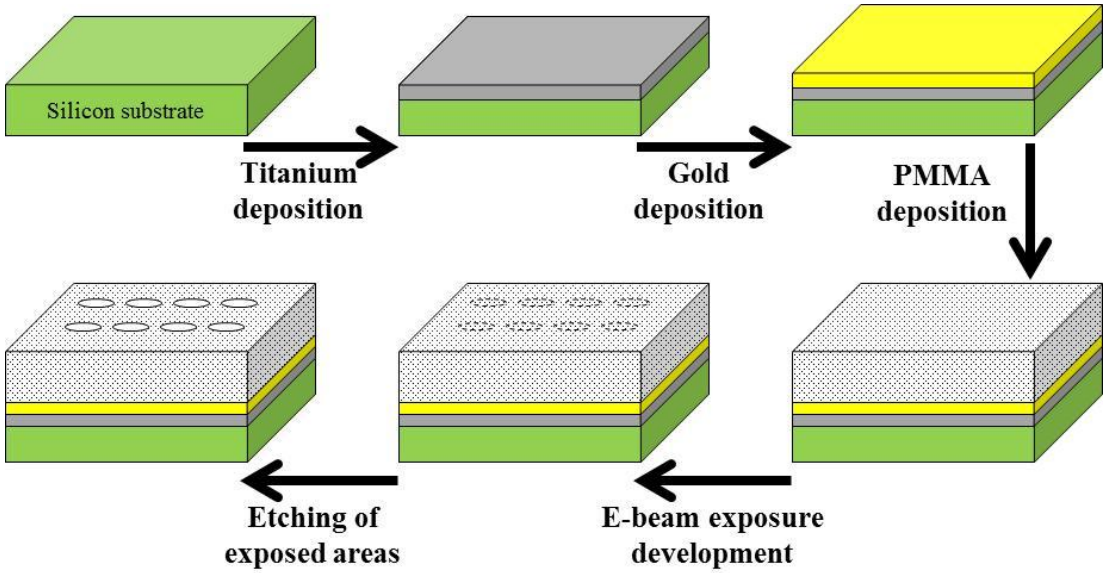

Figure 2.2: Schematic of the steps used to fabricate the template to be electroplated with Rh nanopillars.

Preparation of the substrate began with a (0 0 1) silicon wafer, on which a 20nm thick titanium layer was deposited to act as adhesion layer. Then a 100nm gold layer was deposited by electron beam evaporation to act as electrical contact. This Au seed layer had a columnar grain structure with a <1 1 1> texture and an average grain width larger than all fabricated Rh pillars. Then the substrate was covered with a positive PMMA resist by spin coating. The PMMA was developed by Leica EBPG 5000+ electron beam lithography system operating at a 100 kV acceleration voltage to develop the desired pattern/holes. Finally, the PMMA was immersed in etchant to strip off the developed sites, leaving the desired pattern.

For other electroplating setups, the recipe was provided by the supplier (Technology without Limits, Inc.). Two electrodes configuration was used. The anode used was an insoluble 2×3 $inch^2$ platinized titanium from Stan Rubinstein Association, Inc. As the chip was virtually non-conductive, because of the outermost resist coat, it would not act properly as a cathode. Therefore, another chip was used to act as a cathode to complete the circuit. This additional chip was a one square centimeter gold chip, called a "dummy" chip. To distinguish between the chip that has the array and the other, the former will be called the "real" chip as opposed to the "dummy". To allow electricity to reach the underlying gold layer, the real chip was scratched at a position away from the array in order to strip off the PMMA at that position to ensure the connectivity of the underlying gold layer with the solution, so as to facilitate the reduction process. To confirm electrical connectivity, the chips were connected to an ammeter with one tip contacted with the edge of the real chip (to touch the side of the Au layer) and the other with the dummy chip.

The aforementioned electrodes were immersed in Rh salt solution. The solution was brownish yellow rhodium sulphate, $Rh_2(SO_4)_3$, with a concentration of 2 g/L (Technology without Limits, Inc.). The solution has very good throwing power and excellent coverage and distribution ability and produced white plating deposits.

After pouring the solution into the 250 ml beaker, almost half of the anode and all of both chips were immersed in the solution. The beaker was put in a water bath on top of a hot plate to heat the solution to 35 °C. Plating at an elevated temperature was used to ensure homogenous filling of the pattern, rather than a high initial current pulse as applied by

others- see [30] as an example. The circuit was then connected to start the electroplating, while the solution was mechanically stirred with a magnetic stir bar.

To determine the size effect on the Rh nanopillar properties, four different pillar diameters were chosen to see how the properties were influenced by size reduction. The height to diameter aspect ratio was chosen to be less than or equal to 3:1 (the aspect ratio choice will be discussed in detail in a following sections.) The plating conditions for each pillar size (i.e. diameter) with a constant voltage of 11 V are shown in Table 2.1.

Diameter (nm)	Temperate (°C)	Current density (mA/cm^2)	Plating time	Average height:diameter aspect ratio
125	33	9.11	45 sec	3.9
205	35	9.10	1.5 min	2.5
535	35	9.8	2.5 min	2.3
1135	36	9.1	7.0 min	2.75

Table 2.1: Selected electroplating conditions for each fabricated size. Note that for the 125nm diameter, an aspect ratio greater than 3:1 did not cause the pillars to buckle or to fall.

After turning off the current, the chips were transferred to a solvent (acetone) petri dish for 20 minutes to dissolve the PMMA from the chips (dissolving time is an estimate), followed by 5 sec rinse with isopropyl alcohol (IPA). Figure 2.3 illustrates the process.

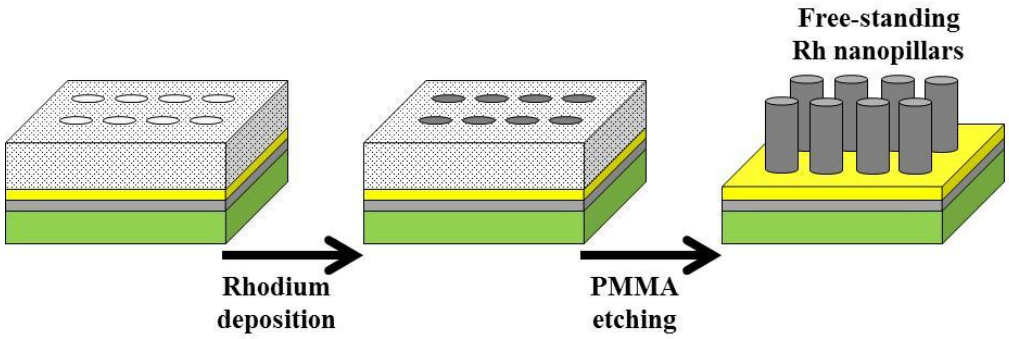

Figure 2.3: Schematic of the etching of the PMMA pattern and how it leads to the free standing pillars.

As the PMMA dissolved, the pillars were exposed and ready for the compression tests. A representative image of each pillar is shown in Figure 2.4.

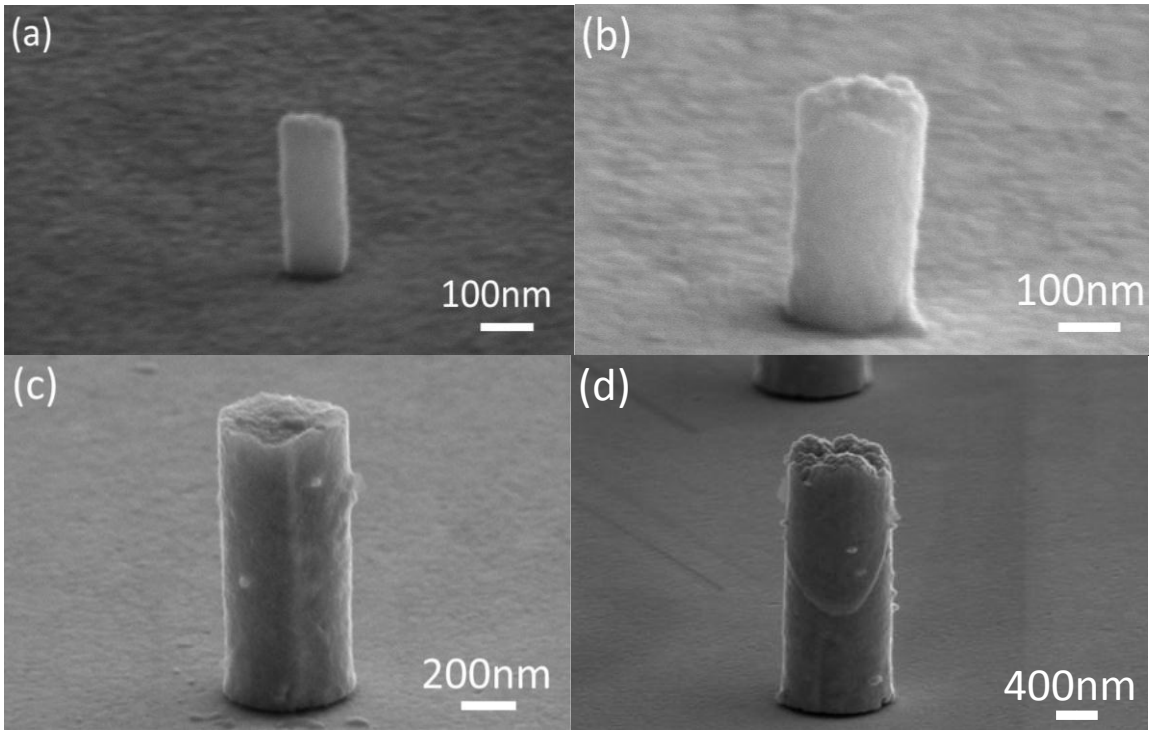

Figure 2.4: SEM images for representative nanopillars, (a) 125nm, (b) 205nm, (c) 535nm, and (d) 1135nm diameter, before compression.

2.2. Testing

2.2.1.Scanning electron microscope (SEM) imaging

Before performing the compression test, the array was imaged under SEM to choose the pillars that are suitable to be compressed. The criteria for a good pillar were as follows:

1- To be free of cracks. All pillars did not have cracks except some of the 535nm sample. This is not due to the diameter size; rather, it may be due to some fabrication variation. Regardless, such cracked pillars were excluded. Figure 2.5 shows a cracked pillar that was excluded from testing.

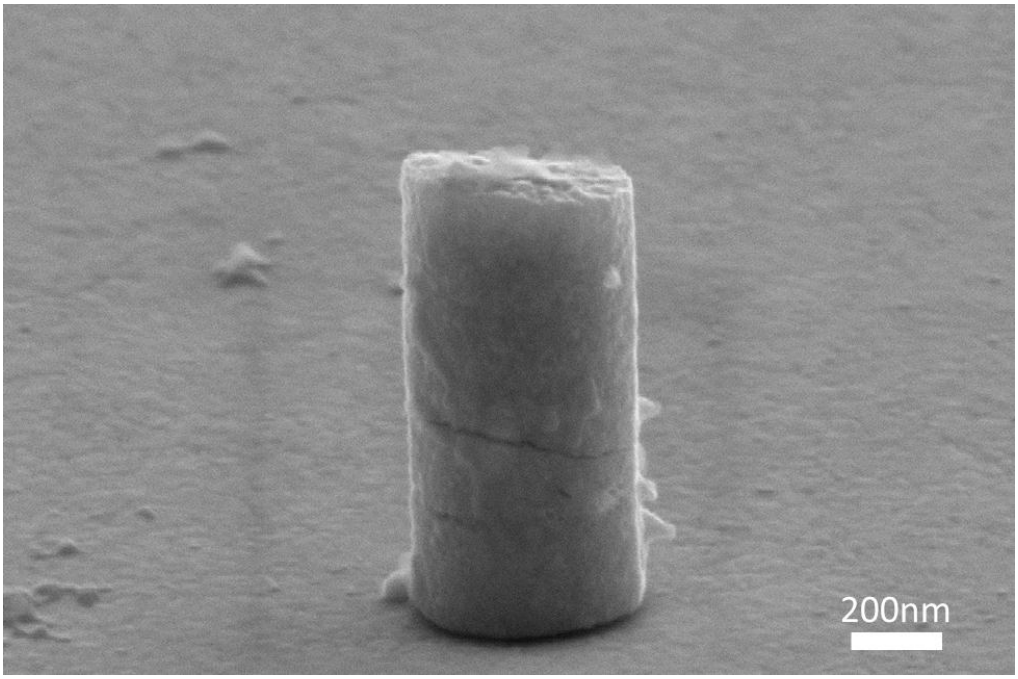

Figure 2.5: 535nm cracked pillar.

2- To have 3:1 (or lower) height to diameter aspect ratio. More precisely, the best height to diameter aspect ratio range was 2.5:1 to 3:1. This aspect ratio range was chosen as a rule of thumb based on our experience in the lab with previous tests

for several materials such as In, Sn, Bi, Pd, and Co [30, 60-63]. Pillars with aspect ratio higher than 3:1 will most likely buckle or fall down as shown in Figure 2.6.

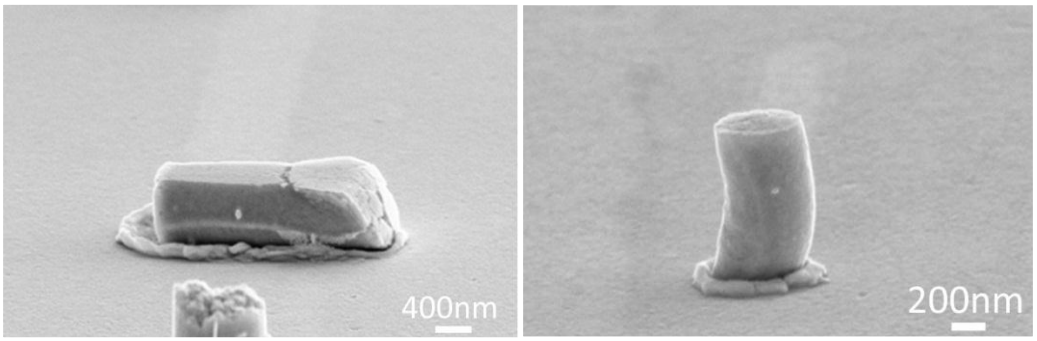

Figure 2.6: A 1135nm pillar that fell down (left) and a 535nm pillar that buckeled (right) as a result of the large height to diameter aspect ratio.

The used SEM was Gemini LEO1550. An angle of 70° was chosen to image the pillars as shown in Figure 2.7.

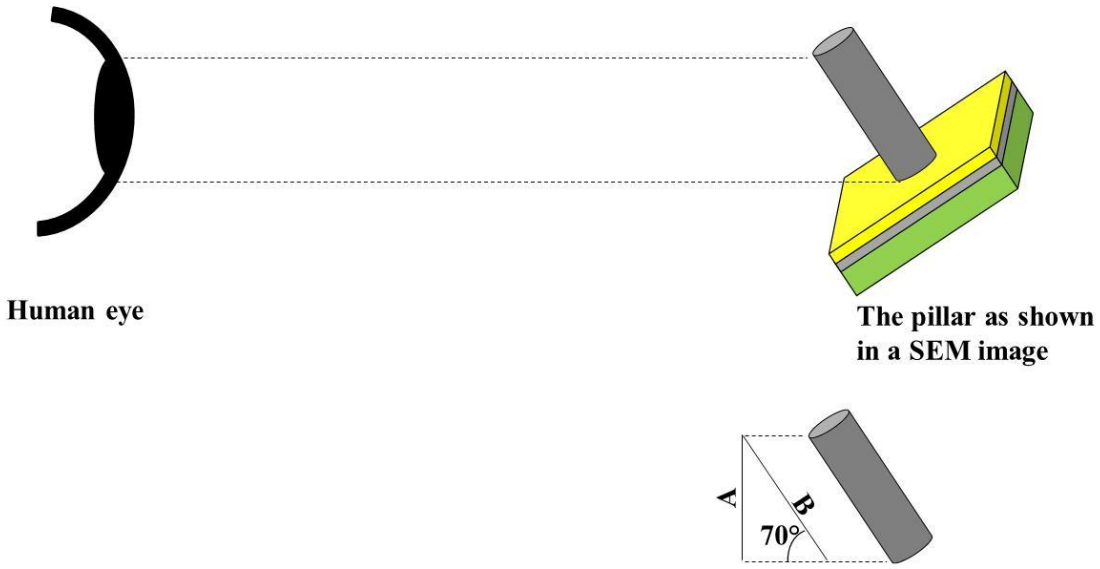

Figure 2.7: An image for a fabricated pillar and how it is seen in the SEM images. The length A represents the observed or measured height as seen in the SEM images where B is the actual or real height of the pillars. Note the 70° tilt angle.

The pillar heights were calculated using the following equation to account for the tilt angle:

$$Actual\ pillar\ hieght = \frac{The\ pillar's\ hieght\ in\ the\ SEM\ image}{\sin(70)}$$

Equation 2.1: The correction equation for the pillars' height by accounting for SEM tilt.

To ensure that the real height was used for analysis, both "measured height" and "actual height" were printed on each image to avoid any confusion as shown in Figure 2.8. Moreover, the diameter was averaged from two values: the diameter at the center and at the bottom of the pillar.

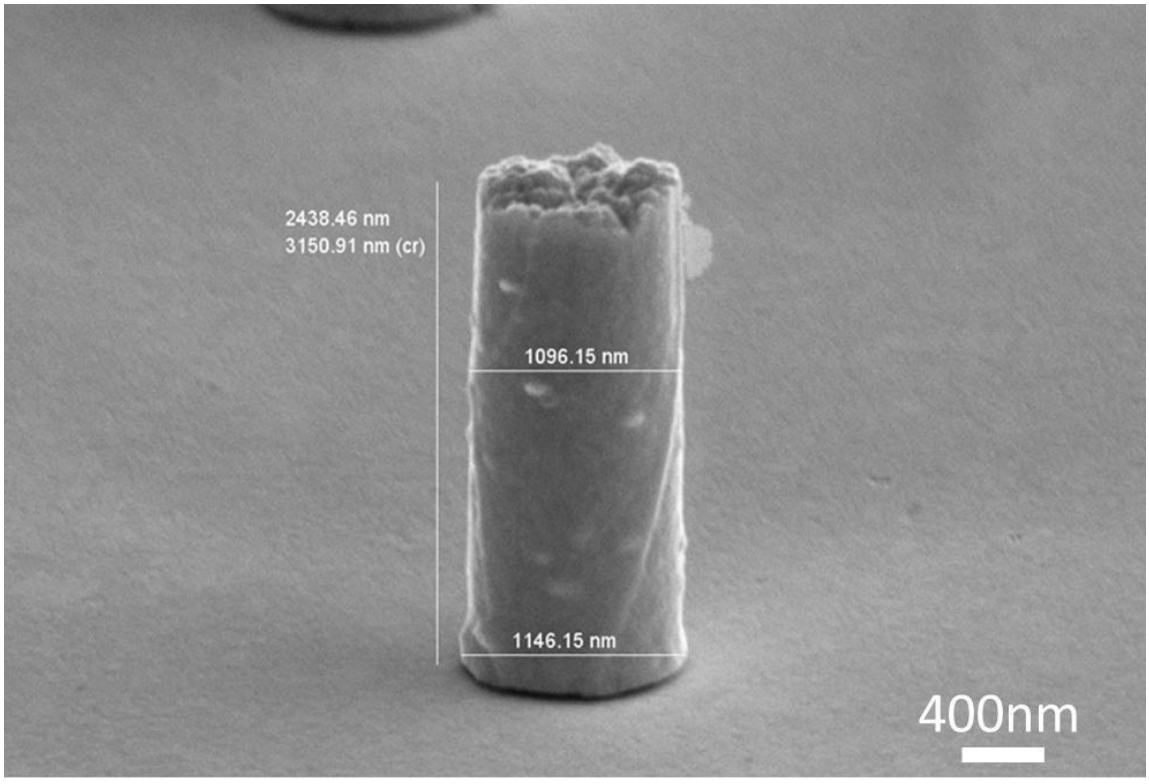

Figure 2.8: Measured and real heights as shown in an image of 1135nm pillar. The "cr" means "corrected".

For each sample or chip, all pillars heights were mostly equal. Moreover, the plating was highly uniform – most of the pattern holes were filled with Rh as shown in Figure 2.9.

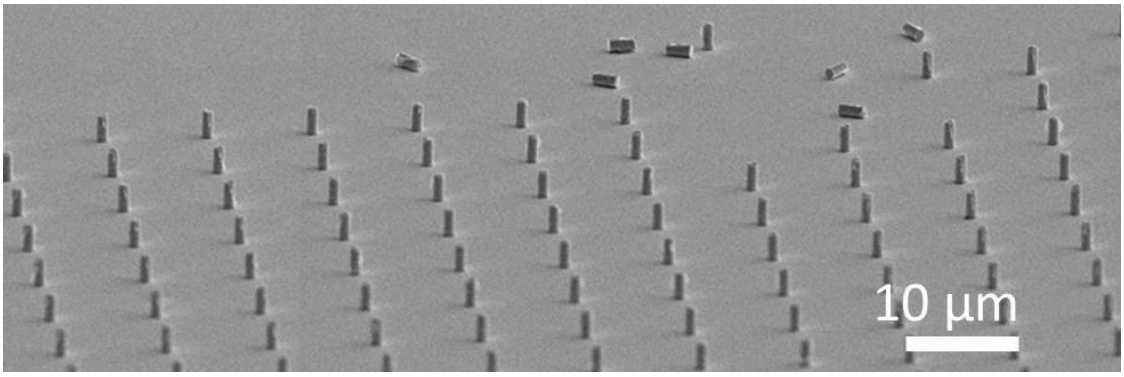

Figure 2.9: SEM image of the 1135nm pillar sample showing the high uniformity of the plating process -all holes were filled in addition to the nearly uniform height of all pillars.

Such uniformity is not present in other materials tested in our lab thus far. A reason for this might be the higher temperature of the Rh plating (35 °C), whereas other materials were plated at room temperature.

Interestingly, most of the 1135nm pillars had "wing" morphologies as shown in Figure 2.10.

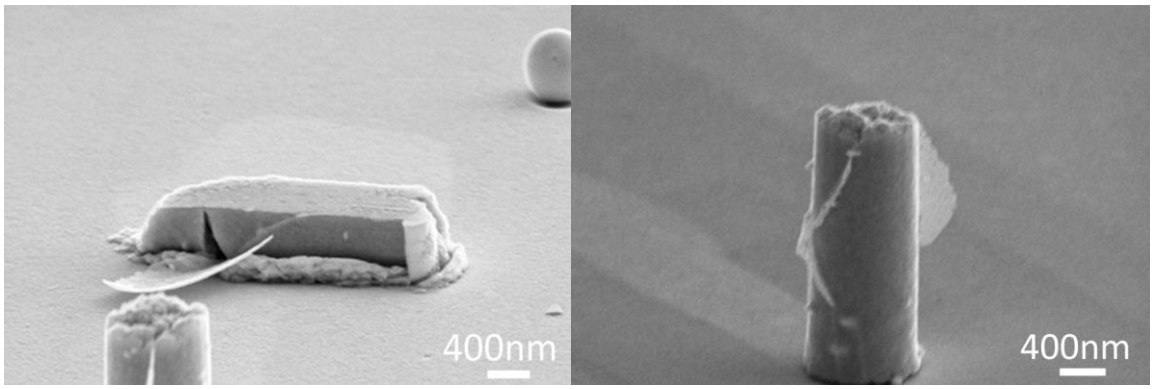

Figure 2.10: Side and front views of the "wings" that appeared in the 1135nm sample.

The TEM and EDX analyses of these wings showed that these wings are composed mainly of Rh as shown in Figure 2.11.

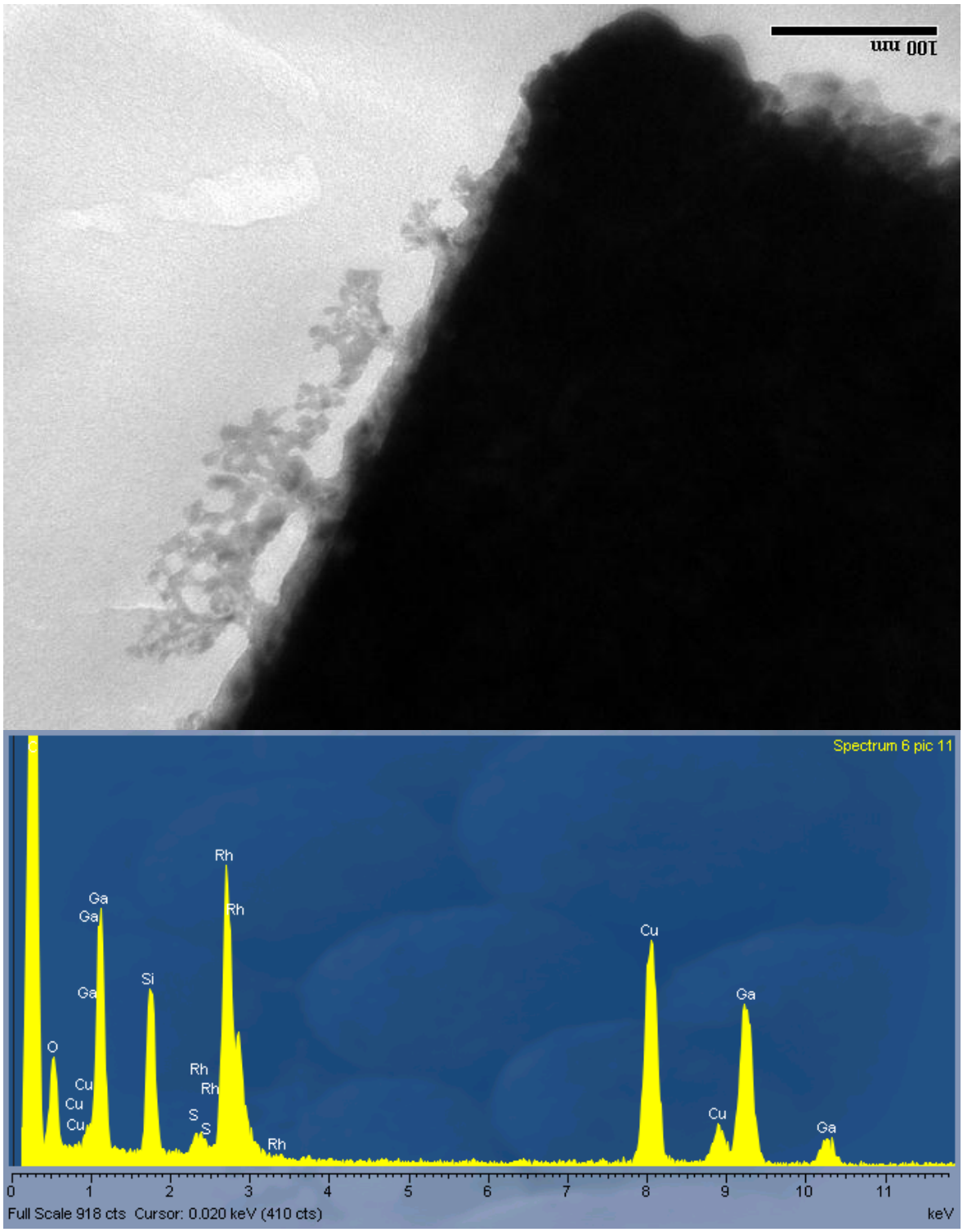

Figure 2.11: TEM image of a wing and its corresponding EDX spectrum. Note that Ga is introduced during the TEM sample preparation.

The cause of the wing formation in the 1135nm-diameter pillars is not clear. One possible reason might be relating to the presence of grooves/trenches in the PMMA patterned holes. Another reason might be due to the stress caused by the rhodium atoms as they wanted to grow laterally. Whatever the reason was, these wings appeared to have no effect on the mechanical properties of the pillars.

2.2.2. Uniaxial compression testing using nanoindentation machine

The uniaxial compression tests were performed *ex situ* with the dynamic contact module (DCM) of a nanoindenter (NanoIndenter® G200, Agilent Technologies Inc.) that has an 8 μm x 8 μm diamond flat-punch indenter tip. These compressions tests were performed with nominal strain-rate control, whereby the assigned displacement rates were maintained through an internal feedback loop between a voice coil applying a force and a capacitive plate measuring the resulting displacement [64].

As for the choice of displacement rates, one displacement rate was chosen experimentally for each size at a constant engineering strain of 30% throughout all tests. Tests at displacement rates lower than 0.1 nm/s were not attempted, as they will not provide reliable results [64]. The 1135nm diameter sample took the longest time to determine an appropriate displacement rate; nine displacement rates were tested and only one gave neatly compressed pillars. After more than 240 successful compression tests, one displacement rate for each size was found to be the suitable, resulting in 4 to 5 successful compressions per data point. The displacement rates that were tested are given in Table 2.2.

Pillar diameter	The chosen displacement rate (nm/s)	The successful test
1135nm	1.0	
	0.5	
	7.0	
	15	
	30	
	0.3	
	3.0	√
535nm	2.0	√
205nm	0.2	
	15	
	1.5	√
125nm	0.1	
	10	
	1.0	√

Table 2.2: Different displacement rates for each diameter, noting successful ones.

The strain rate sensitivity was neglected for two reasons. First, the yield stress here is independent of strain rate (and displacement rate) as there are no upper yield and lower yield points, as is the case when the yield points become strain-rate dependent [59]. Second, it has been proven that metals tested below 0.3 T_m (T_m = melting temperate) become independent of strain rate or displacement rate, [59] which is obviously the case here, as room temperature is much lower that 30% of the melting temperature of Rh. Consequently, different rates were chosen for different sizes.

3. Results and Discussion

3.1. Effect of Fabrication Method on Determining the Nanomechanical Properties

The effect of the fabrication method of the pillars, FIB or electroplating, on the attained size effects is debatable: some researchers state that an effect does exists [31, 65] while others say it does not –including some who initially believe there was an effect but changed their opinion [66-69]. The greatest concern is the Ga^+ ion penetration from the FIB into fabricated pillar. It is highly probable that the latter opinion, fabrication method does not effect, is the correct as the findings that support it are the up-to-date for fcc metals and bcc alloy systems. Such findings confirm that for fcc materials and bcc alloy systems, the size effects are a strong function of initial dislocation density rather than the fabrication method [64]. This means that the Ga^+ ion beam has no effect on the pillars. Therefore, the above conclusion about the effect of the fabrication method holds true only when the FIB and electroplated pillars are identical in shape and structure. For example, higher aspect-ratio FIB pillars have a taper (see Figure 3.16) that will make the results differ from that of the electroplated pillar of the same material and structure, because of the non-uniform load distribution along the pillars caused by the taper.

3.2. Pre-deformation or Substrate Effect on Determining Nanomechanical Properties

The size effect in this study was investigated only in the plastic region of the stress-strain curve. The elastic region was not investigated because the substrate effects occur fully in the elastic region. In other words, as titanium and gold, the substrate materials, are softer

than rhodium, their elastic and plastic deformation and failure will occur while rhodium is still elastically deforming (note that the three materials share the same curve). Figure 3.1 shows a rhodium pillar sank into the adhesion layer.

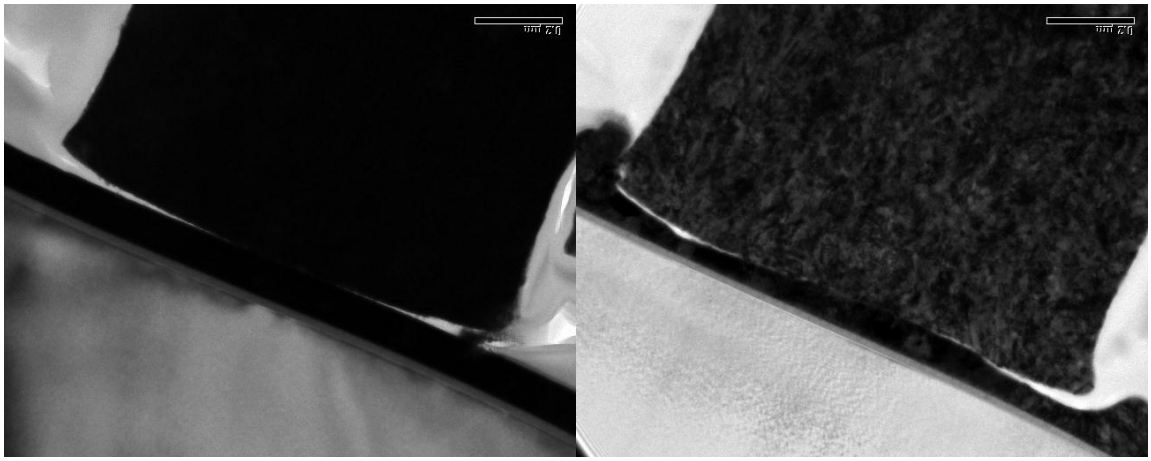

Figure 3.1: The pillar before (left) and after (right) compression. Note how the adhesion layer popped up or bulged from both sides of the bottom of the pillar.

Therefore, it is difficult to exclude the substrate (i.e. Au and Ti) effect in the elastic region of the curve. Therefore, the slope of the elastic region of rhodium stress-strain curve is not young's modulus of the nanoscale rhodium. Instead, it is the "effective" young's modulus of Rh, Au, and Ti combined which does not serve the goal of this study. Consequently, it is safer to begin exploring the nanomecahnical properties of Rh from the yield point that is expected to be the same for the curve of Rh that is on top of Au and Ti and of the curve of hypothetical Rh that is on top of Si (Si is harder than Rh). Figure 3.2 illustrates the aforementioned identical yield points.

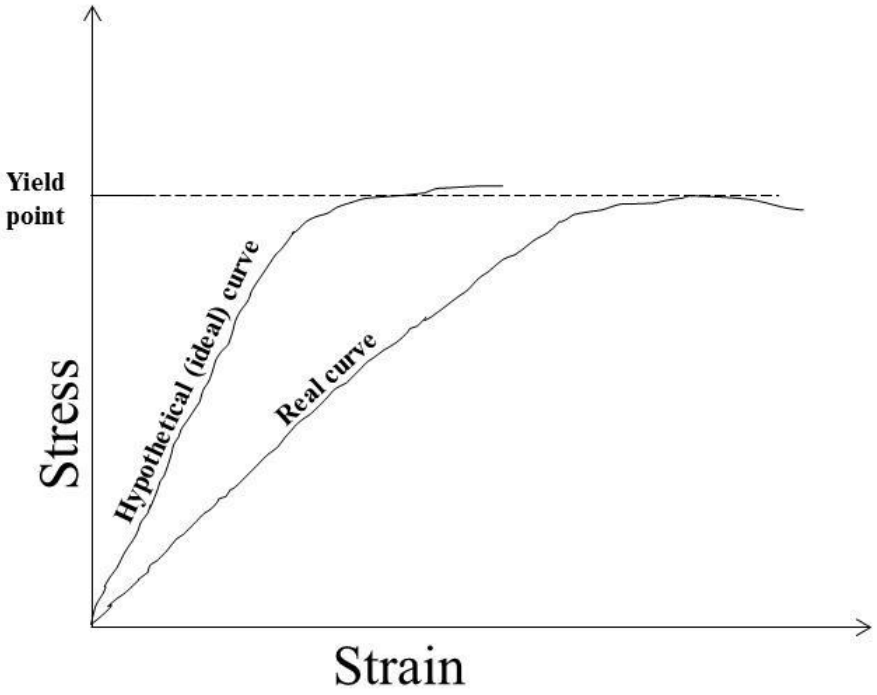

Figure 3.2: Pure Rh and Rh with substrate effect curves. Note that both curves share the same yield point. Such explanation needs more investigation for further evidence.

Before obtaining these values from the stress-strain curves, the deformation steps should be investigated, because these yield points cannot be directly extracted from the curves, as will be shown.

As described above, the Rh pillars are standing on gold and titanium layers that are on top of the Si substrate. As Rh is much harder than gold, the Rh pillars will sink into the gold and titanium with virtually no deformation before reaching the Si substrate, after which it starts deforming. Therefore, the deformation steps are as follows: (1) Alignment between the indenter and the pillar's top surface [32], (2) the Rh pillar sinks into the gold and titanium with virtually no deformation (for the 125nm sample, the pillars deform without sinking due to the weakening effect discussed later,) (2) the Rh pillar reaches the

Si substrate, and finally (3) the Rh pillar starts deforming (because silicon is harder than Rh).

The first step causes what is called pre-deformation effect. This effect is manifested on the stress-strain curves in the nonlinearity at the onset of the curves, as shown in Figure 3.3.

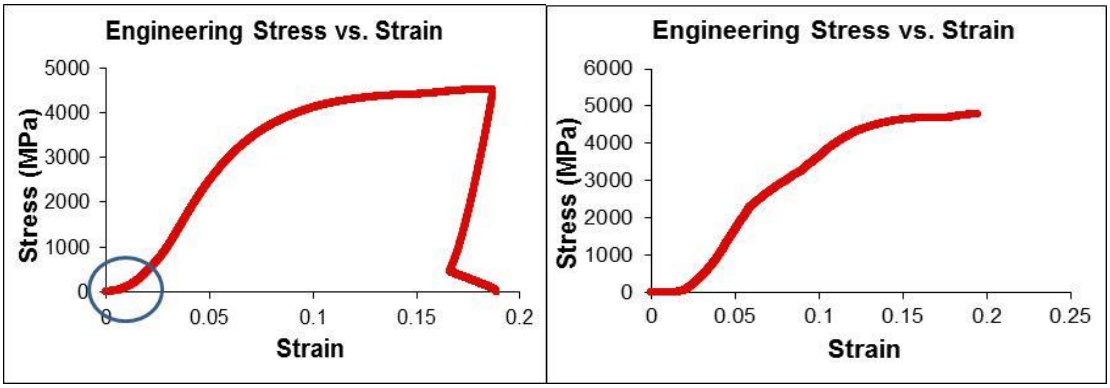

Figure 3.3: The pre-deformation effect on the stress-strain diagram for 1135nm (a) and 535nm (b). The effect gets clearer for small sizes.

Moreover, the stress-strain diagrams for the 535nm sample showed an interesting effect of the aspect ratio on this nonlinearity. When the pillar aspect ratio was relatively high, the pre-deformation effect disappeared after smaller amounts of strain whereas when the pillar has a low aspect ratio, the pre-deformation sustains more strain before the onset of the elastic part of the stress-strain curve. This aspect ratio effect is shown in the Figure 3.4 for the 535nm sample. The 535nm sample was chosen to prove this effect because it was the only sample that had pillars that differed in height; pillars on other samples (1135, 205, 125nm) had similar heights throughout the chip.

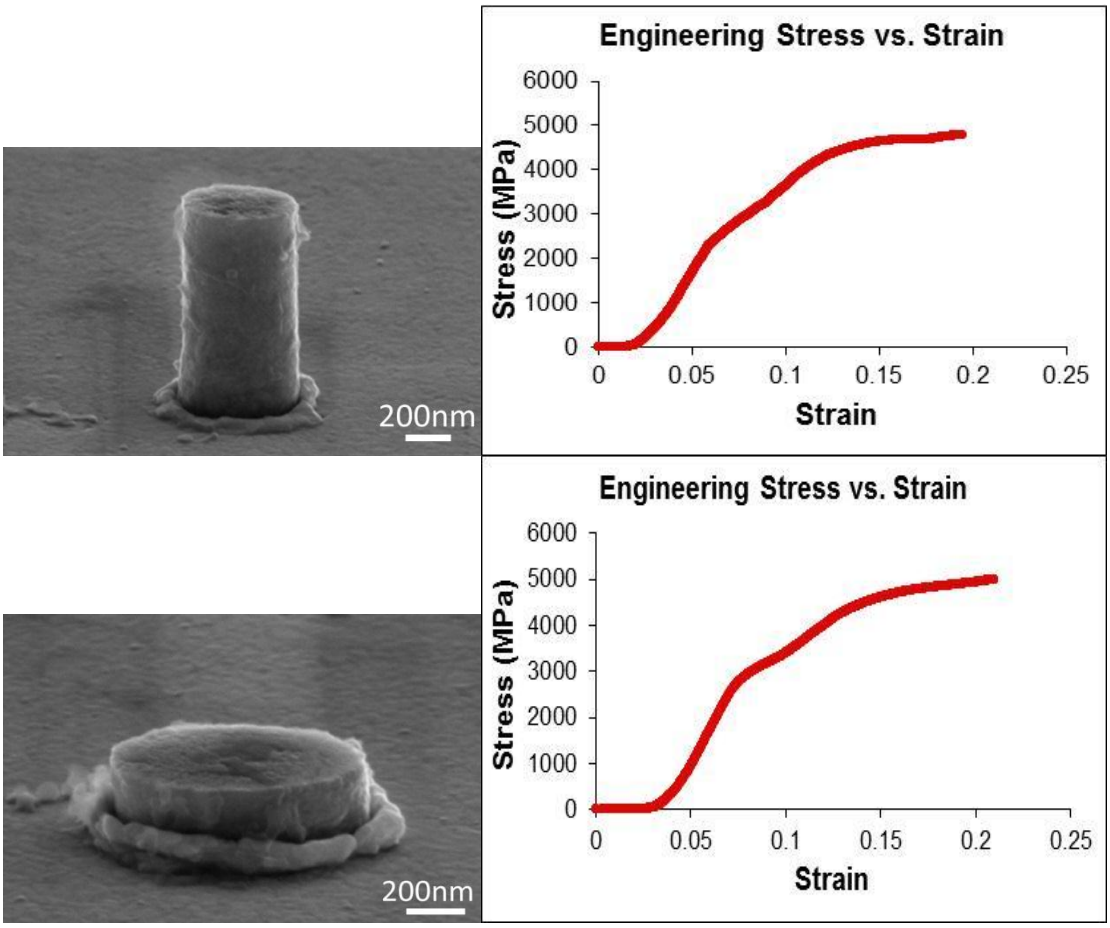

Figure 3.4: Aspect ratio-pre-deformation relation for two 535nm diameter pillars; the lower the aspect ratio the greater the pre-deformation effect, prior to the onset of the elastic region.

As this pre-deformation effect is present, the widely standard method of locating the yield stress at 0.2% off-set strain does not work directly here because the 0.2% method assumes no pre-deformation effect. Therefore, another method must be devised to account for and eliminate this effect. One method is to shift the origin, (0,0) point, to the end of the pre-deformation curve, and then the 0.2% strain parallel line could be drawn. The problem, however, with this method is that it does not eliminate the pre-deformation effect as there is no clear cut for the end of the pre-deformation effect. Another possibility is to draw a parallel line at a value other than 0.2%. Many researchers selected their own values with different reasoning for their selection, though these reasons were

not convincing or applicable for the present study. The selection included values such as 10% or 7.5% strains [64, 70]. This method is not practical too because of the same problem of the first one: the difficulty to make a clear cut for where the substrate effect ends. To the best of our knowledge, the best method is another method in which two lines are drawn tangent to the first two plateaus in the curve where the intersection of these lines is the yield point. Figure 3.5 shows an example from each size.

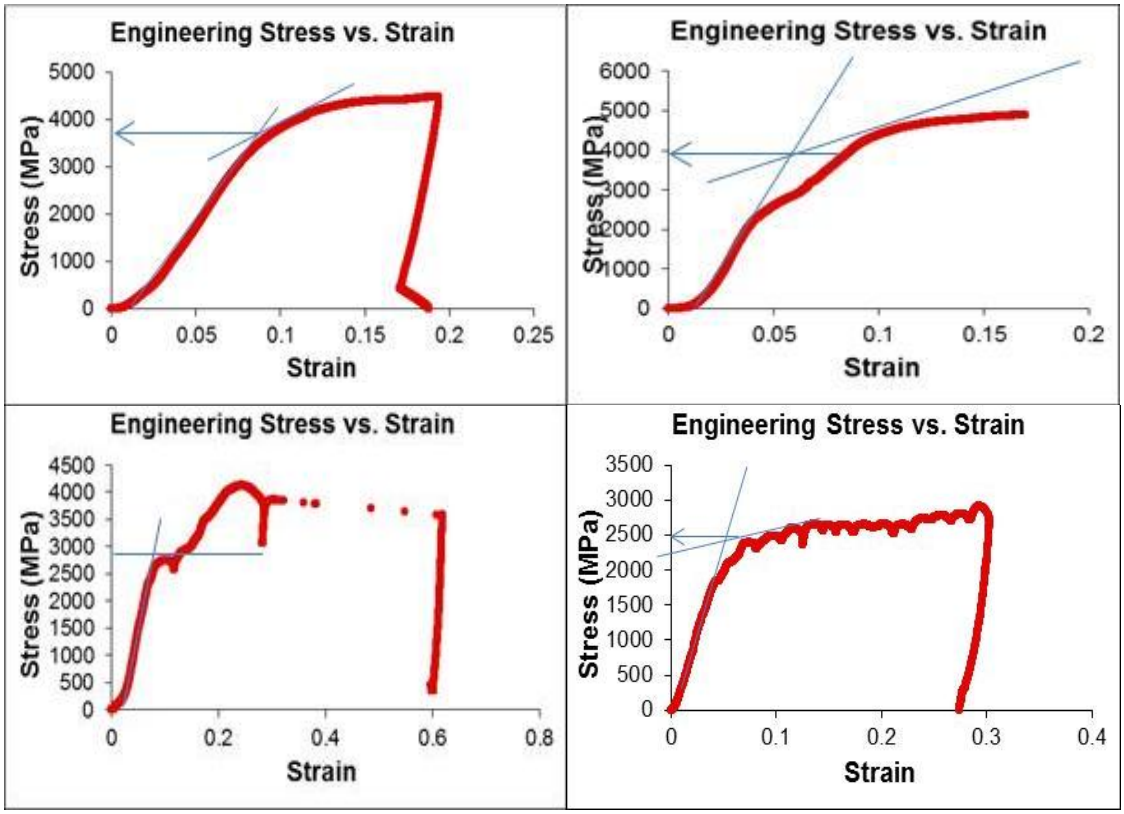

Figure 3.5: Representative stress-strain curves for 1135 (top left), 535 (top right), 205 (bottom left), and 125nm (bottom right) diameter pillars, where the yield point is the intersection of the two blue lines.

This method may be called "two lines method." Noticeably, for each size the method gave yield stresses with which corresponding strains are close in value. Table 3.1 shows the yield points of selected pillars for two sizes and their corresponding

strains and how a deviated yield point turned to have a corresponding strain that is not compatible with the rest of strains for other pillars.

Pillar Size/Diameter (nm)	Yield Point (MPa)	Corresponding Strain	Pillar Size/Diameter (nm)	Yield Point (MPa)	Corresponding Strain
535	4684	0.116 ≈ 0.12	125	2001	0.058 ≈ 0.06
	4159	0.2		2235	0.065 ≈ 0.07
	4478	0.132 ≈ 0.13		2706	0.117 ≈ 0.12
	4599	0.119 ≈ 0.12		2110	0.084 ≈ 0.08

Table 3.1: Selected pillars yield points with their corresponding strain. The method for determining the yield points works by indicating that any unusual yield point for a pillar corresponds to an unusual strain leading to rejection of such a pillar. The highlighted values are the unusual ones.

3.3. TEM and EDX Analysis

TEM imaging was taken in The Canadian Centre for Electron Microscopy (CCEM) at McMaster University. Figure 3.6 shows two TEM images of 1000nm Rh nanopillars before and after compression.

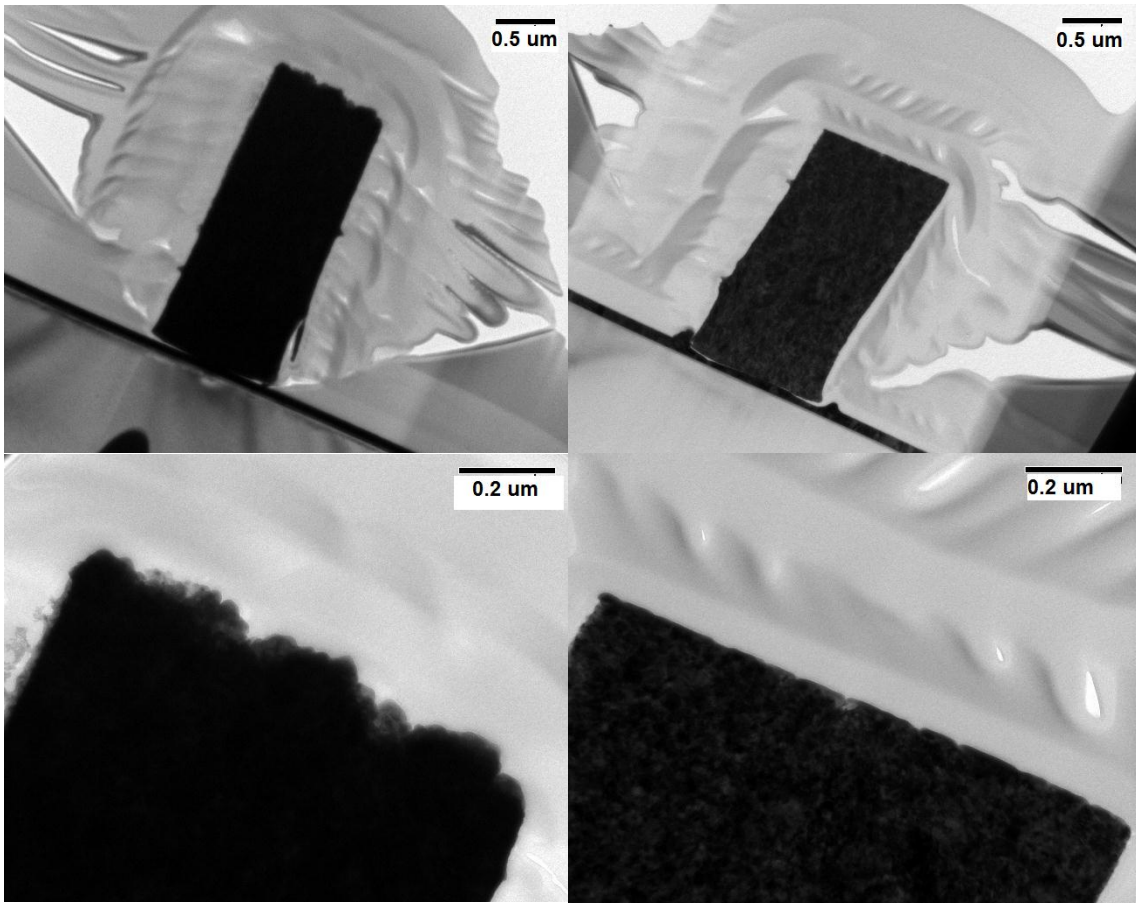

Figure 3.6: Images with different magnifications for 1000nm Rh pillars before and after compression. (Top left) Rh nanopillar before compression. (Top right) Rh nanopillar after compression. (Bottom left) A high magnification image of the top of an uncompressed pillar. (Bottom right) Close image for the top of a compressed pillar.

The ebeam diffraction and a high magnification TEM images show that the pillars have a nanocrystalline structure. Figure 3.7 is electron diffraction patterns of 1000nm Rh pillar before and after compression. Note that the compression did not change the nanocrystallinity of the pillars.

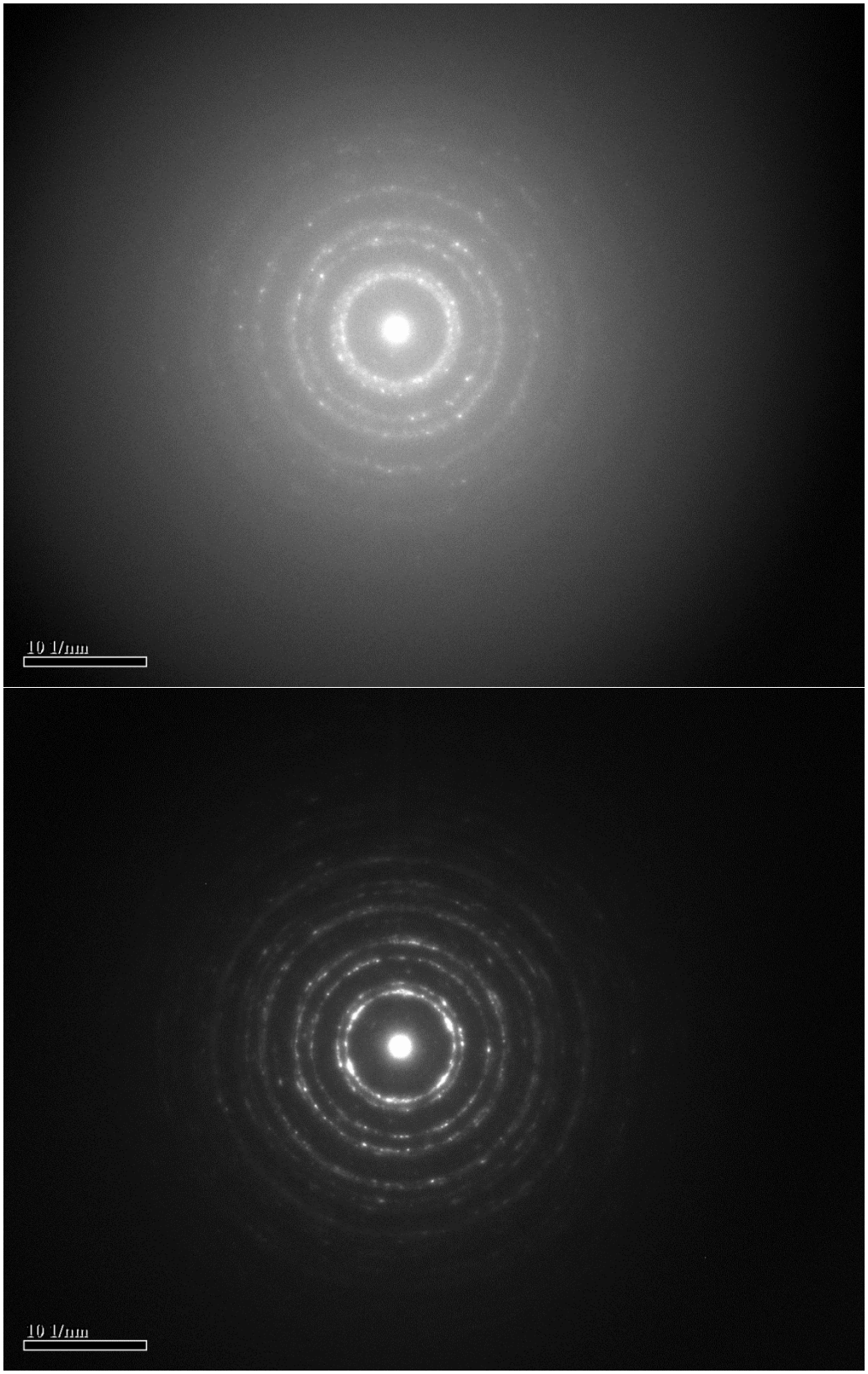

Figure 3.7: Electron beam diffraction for 1000nm Rh nanopillars before (top) and after (bottom) compression. Note that there is no significant microstructural change due to compression.

Figure 3.8 is a high resolution transmission electron microscopy (HRTEM) “nanograph” for a 1000nm pillar that also shows the nanocrystallinity of the pillars.

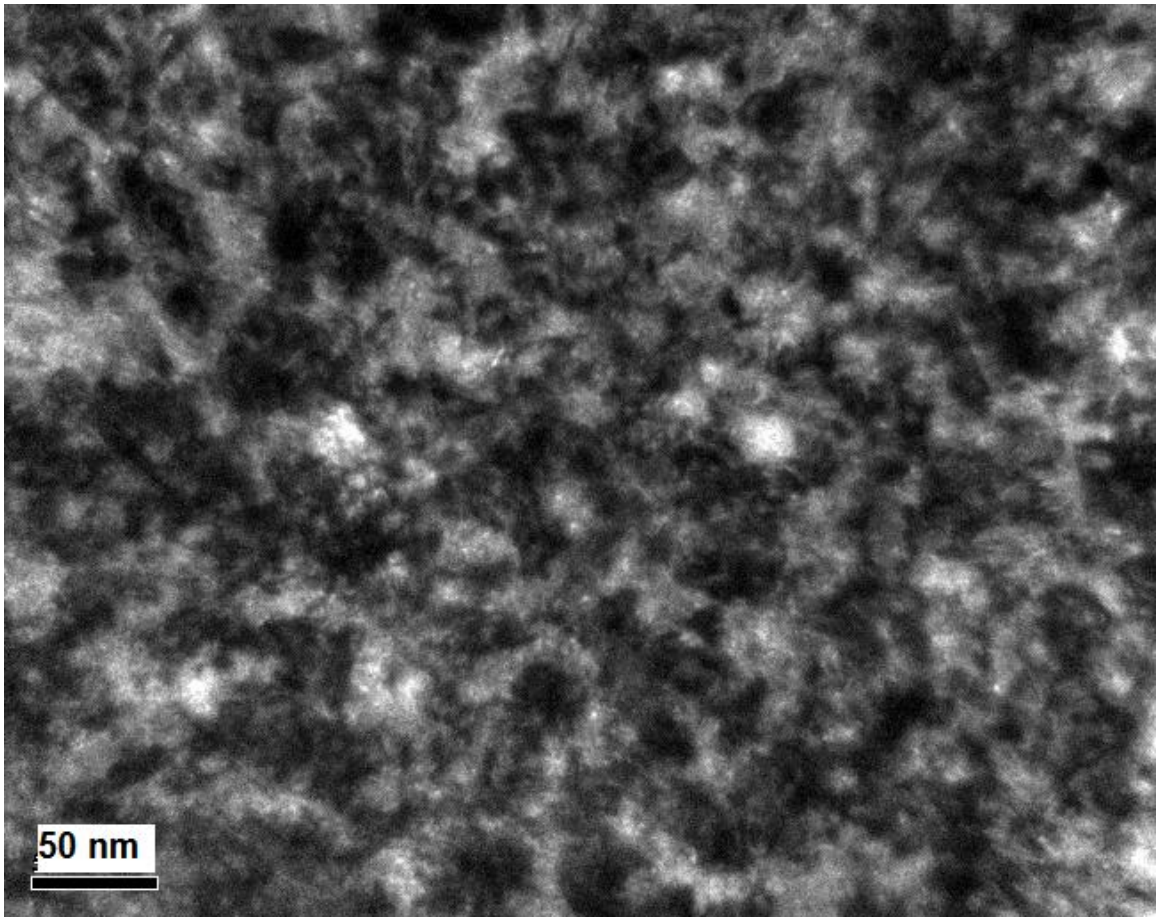

Figure 3.8: HRTEM “nanograph” for 1000nm Rh nanopillar after compression. Different white, black, and grey regions indicate different grains. The color difference is due to different orientations of these grains.

The nanocrystallinity is also evidenced by SEM as shown in Figure 3.9.

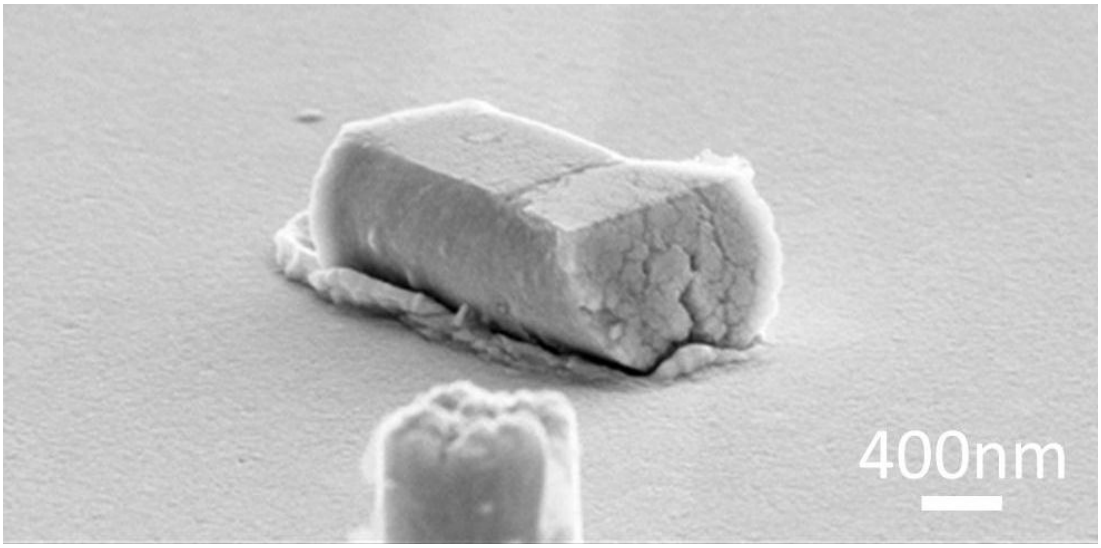

Figure 3.9: SEM image showing the nanocrystalline nature of electroplated Rh nanopillars.

The spectrum of the pillars showed that Rh pillar fabricated in this study contain mainly thallium (Tl) and copper (Cu) atoms as shown in the following spectrum in Figure 3.10. The source of thallium is unknown.

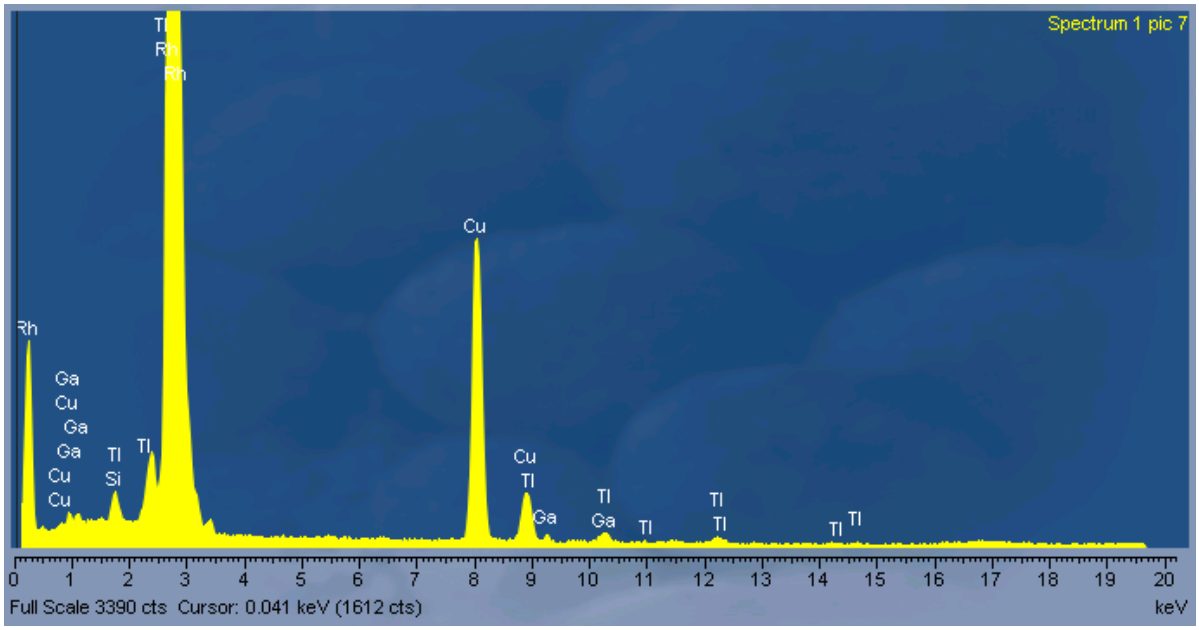

Figure 3.10: The spectrum of the 1000nm rhodium pillars after compression indicating the presence of thallium impurities.

However, thallium is not homogeneously distributed throughout the pillar. Figure 3.11 shows the spectrum of a protrusion where there are no thallium impurities.

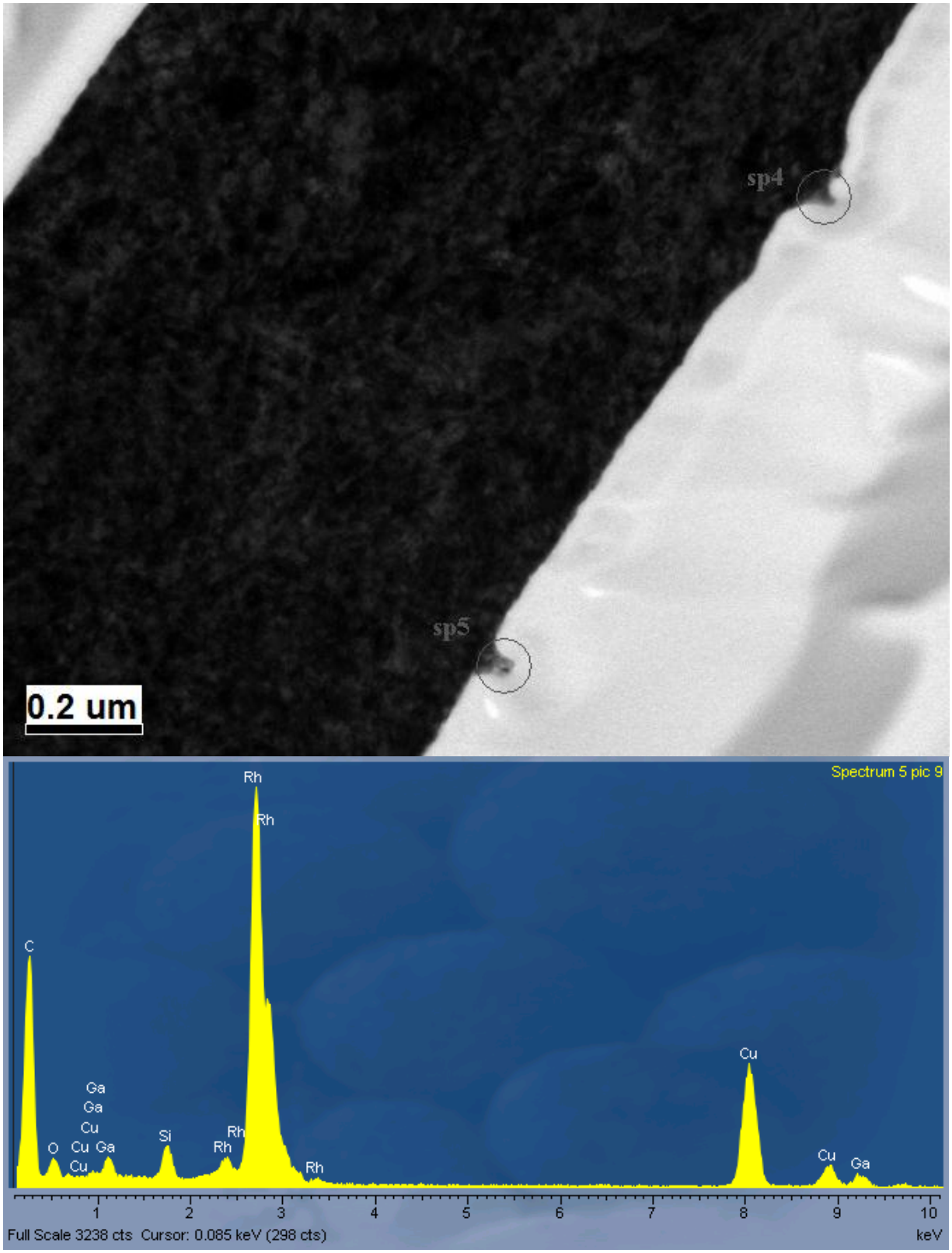

Figure 3.11: TEM image of two protrusions and the corresponding spectrum for the bottom one.

3.4. The Pillars' Size Reduction Effect on the Mechanical Properties of Rh

In general, the size reduction effect on the yield stress cannot be identified straightforwardly due to three reasons. First, the microstructural influence: changing the microstructure changes the size effect completely, in addition to the ambiguity of attributing the acquired effect to either a pristine or to an external source. As mentioned above, the size effect is different for different microstructures: For single crystals with zero or non-zero initial dislocations it has been shown that the strength, or yield point, increases as the external size decreases, [30, 32, 61, 64, 70, 71] whereas, for micro- or nanocrystalline structure it decreases as the external size decreases [72-75]where the grain size becomes comparable with the diameter of the pillar. The latter is the case for rhodium.

In this study, the bulk Rh samples were polycrystalline, [39] which could be considered as a counterpart of the small sized nanocrystalline pillars.

Jang and Greer [75] reported that the strengthening of such nanocrystalline materials scales with the inverse of grain size with a square root dependence down to approximately 20nm grain size, representing the widely known Hall-Petch relation [76, 77].

The second reason the yield stress cannot be identified straightforwardly is the aforementioned difficulty in determining the values of the yield points, as a consequence of pre-deformation and substrate effects.

The third reason is that the bulk sample tests were tension tests, whereas with nanosamples they were compression tests. However, this change is not expected to give any major difference between the obtained values of yield point in both tests [59].

Having chosen and reasoned the choice of the bulk yield point (67 MPa) earlier chapter, and after implementing the aforementioned two-lines method, the values for yield stresses for pillars with diameters of 2.54 **m**m, 1135nm, 535nm, 205nm, and 125nm are, respectively, as follows: 67, 4200, 4600, 2400, and 2100 MPa. As the difference between the values of the yield points of 1135 and 535nm diameter samples was within the experimental error, they could be represented by an average single value of 4400 MPa. The same applies to the 205 and 125nm samples: the value is 2250 MPa. Therefore, this leads to mention that the increment in the value of yield point is per range of diameters rather than per particular diameter. Defining a set of diameter range rather than a particular diameter to represent the stages of size effect is the norm for nanocrystalline materials; precise determination for a particular diameter to represent a transition effect is difficult due to the stochastic nature of these compression tests, combined with the possible uncertainty at initial loading between the pillars and the indenter flat punch [70]. Rather, it is more prudent to identify the transition as a range of diameters rather than a precise diameter [64]. However, this is not the first time that this range-based transition was noticed: Min et al. [78] divided the intrinsic properties into two categories of "additive" and "non-additive" where the additive is the properties given by summing the contributions from the individual atoms or molecules, while the non-additive are properties that depend on cooperative effects from a certain number of atoms or molecules. In the present case, the range may be determined as follows:

X_{bulk} to X_1 nm → X_1 to X_n nm → X_n to 1135nm → 1135 to 535nm → 535 to 205nm → 205nm to $X_{quantum}$, where X_{bulk} is any bulk diameter and X_1 is the transition diameter from bulk to the nanoscale regime that is very difficult to identify. Some researchers assigned a wide range of single values to represent such transition, ranging from values as small as 100nm [23] to values as large as 42 µm [24]. $X_{quantum}$ is the nano- to quantum transition diameter which is much more difficult to determine than X_1, and one of the greatest challenges for modern science [79] though its discussion is beyond the scope of this project.

The interpretation of the yield point change with the size reduction will be discussed in the following section.

3.5. Active Modes and Mechanisms behind the Size Effect

Modes here are the behaviours of microstructural components (i.e. dislocation, grain boundaries, atoms, etc.) of the pillar, while the mechanism here means the scenario of the increasing, decreasing or fluctuating of the values of yield points as the size of the pillar decreases.

There are several possible modes to describe the size effect on nanomaterials. Choosing one mode as being responsible for the size effect is a highly debatable topic [64, 65]. As Rh has a homologous temperature ≈ 0.13 at ambient conditions, all thermally activated modes/processes are excluded, such as diffusion, dislocation climb, etc. [61]. Therefore, among the non-thermally activated modes, the modes that appeared to be compatible with the obtained stress-strain diagrams and SEM images are as follows:

A- Grain boundary-mediated mode.

B- Dislocation-driven mode.

The specific process representing the grain boundary-mediated mode is the grain boundary sliding which is a process that was proven to soften nanocrystalline materials [72-74]. Grain boundary sliding acts as a replacement for the plasticity theory that fails when reducing the nanopillar beyond certain size/diameter. Figure 3.12 illustrates this sliding process. Though nanocrystalline, the deformation of small sized nanopillars in Figure 3.12 appears like that for single crystalline materials. The explanation for this is that as the grain size produced by the electroplating process is independent of the nanopillar size, the grain fraction per unit volume is the same for all pillar sizes. Consequently, larger pillars are completely nanocrystalline in nature while smaller ones behave like a single crystal as the number of grains across the diameter is very few.

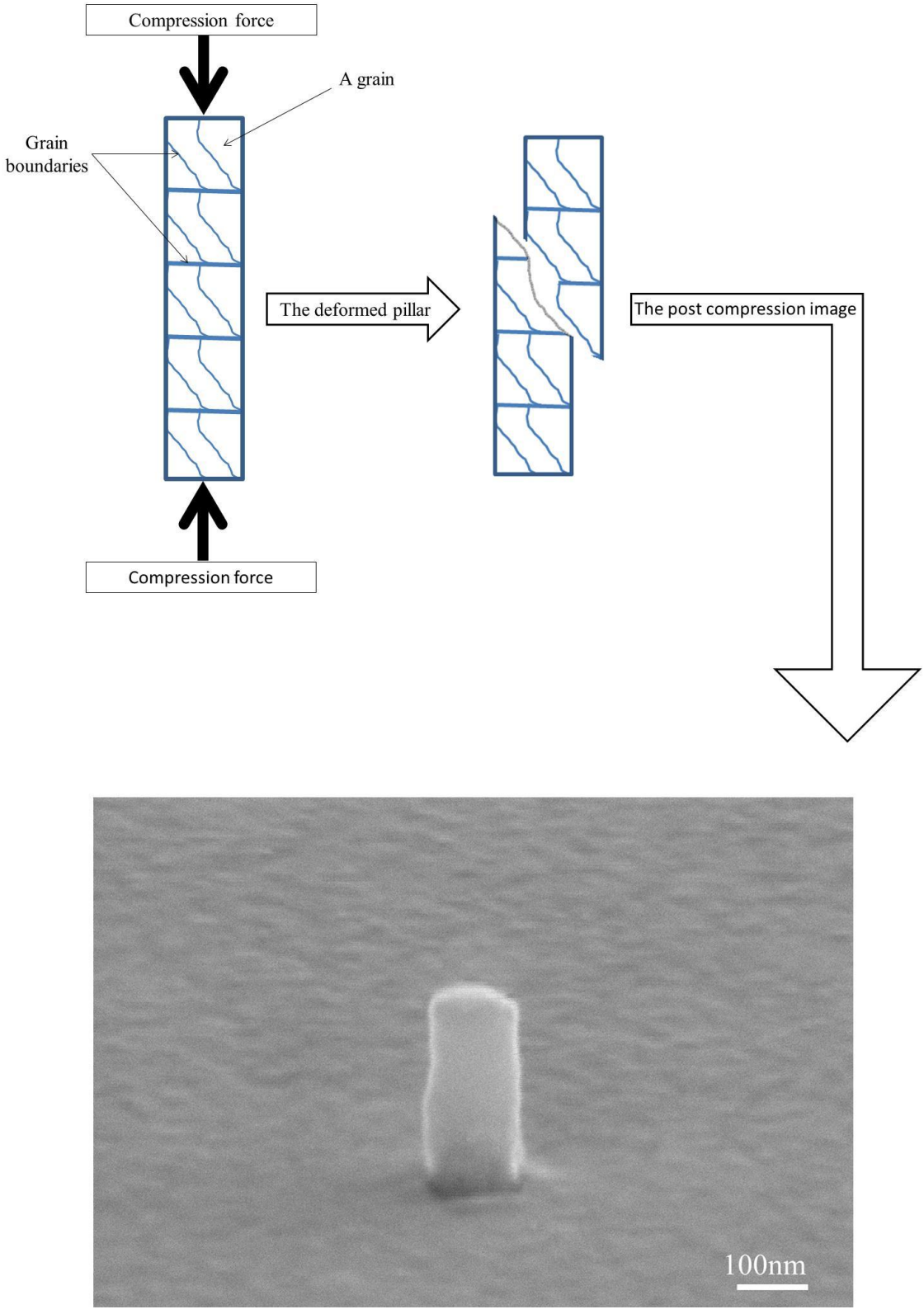

Figure 3.12: Grain boundary sliding process as clearly demonstrated in a 125nm pillar. Although not single crystalline, the deformation looks like that for single crystalline, most likely due to the small size of the grain coupled with the small diameter resulting in a single crystal-like structure.

The SEM image in Figure 3.13 clearly shows the grain boundary sliding (evidenced by the intergranular cracks) when the pillar was mistakenly compressed from the side.

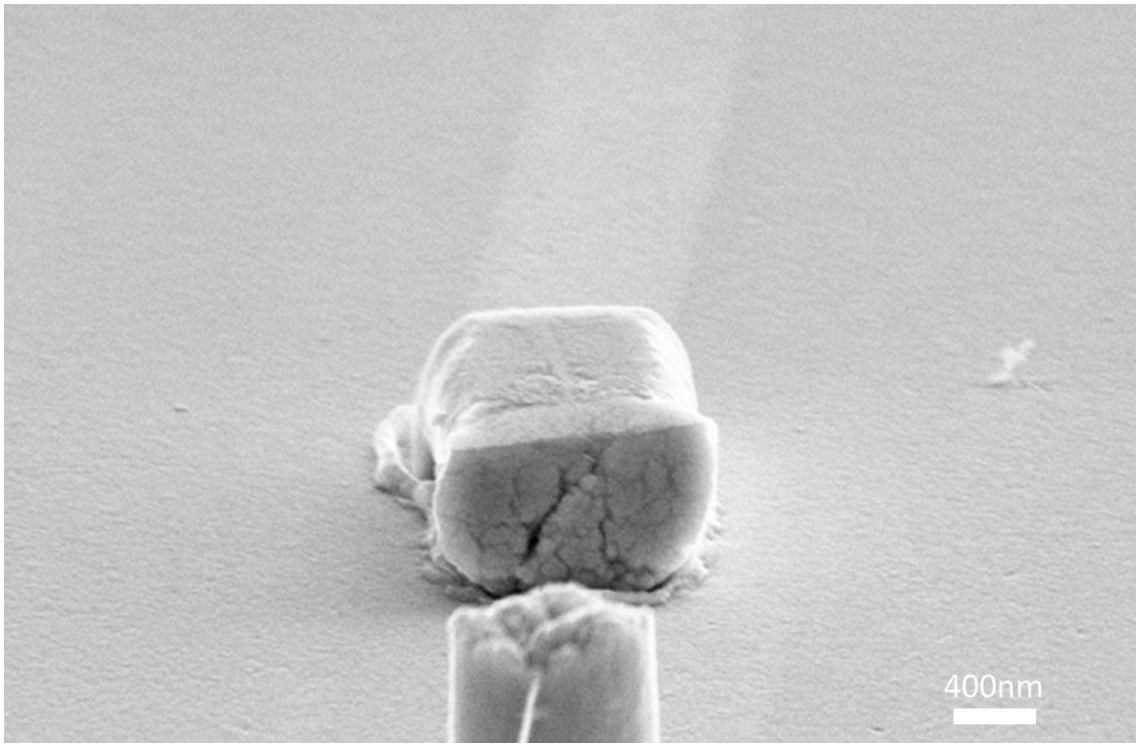

Figure 3.13: Intergranular cracking as an evidence for the grain boundary sliding effect that severely deteriorates the yield point for small sized pillars.

As mentioned above, the dislocation-driven mode is the other mode that acts simultaneously with grain boundary-mediated mode (viz. grain boundary sliding process) in weakening the nanocrystalline materials as the size of the pillar gets smaller. Here, reducing the pillar diameter reduces the number of barriers -grain boundaries and impurities- the dislocations will encounter while moving as demonstrated in Figure 3.14. For the representative pillars in the figure, for the larger pillar the dislocations (that is responsible for the plastic deformation) encounter four barriers (only grain boundaries in this case –no impurities), whereas for the smaller pillar –with the same grain size- the dislocations experience only two barriers, and is thus two times weaker.

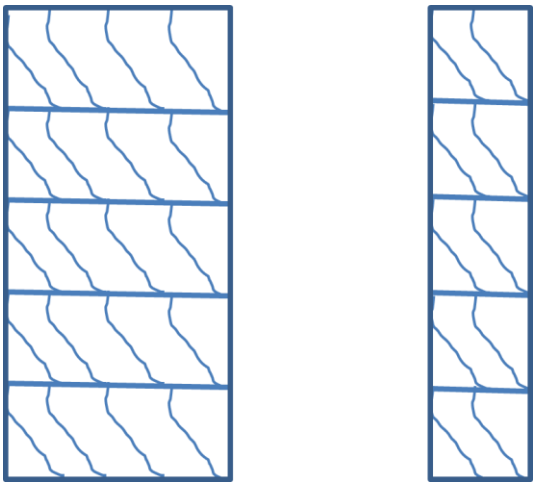

Figure 3.14: Schematic 2D section of two pillars of different size illustrating how the dislocation-driven mode weakens the material due to small grain size coupled with small pillar size.

As shown above, the aforementioned two modes act simultaneously for all sizes. However, for small sizes the grain boundary-mediated mode becomes the predominant deformation mode [80] - this does not mean the other mode, the dislocation-driven mode, is not active; rather, it exists but with a smaller percentage of contribution and mostly at the beginning of the compression/deformation.

In turn, the trend of the size effect on the yield point may be interpreted by either one of three mechanisms or scenarios below. All of the scenarios below share the same overall picture: the strength of the pillars increase up to certain point and then start decreasing. Therefore, all three scenarios share the same size effect after certain diamter -for nanocrystalline Rh: smaller is weaker- and also share the same responsible modes; they only differ in interpreting the dwindling trend. The mechanisms are as follows:

1- The size reduction increases the yield point up to the range from 1135 to 535nm. However, in the range from 535 to 205nm the size effect is reversed: the yield point is decreased as size is decreased because the pillar diameter becomes comparable with the grain size.

2- The second “suggested” scenario is that the size effect holds the same for all sizes: yield point increases with size reduction, but there were some instrumentational and fabrication-embedded variations/problems associated with the small sized pillars, 205 and 125nm, which excluded them from the increasing trend. One of these fabrication-embedded problems was the non-uniformity of the cylindrical shape of the 125 and 205nm pillars as shown in the Figure 3.15. One might say that the magnification is higher for smaller pillars that is why finer details of the walls become visible, while for larger pillars the roughness is not that clear because of the lower magnification. This is partly true, but if we compare the protrusions size to the pillar size, the smaller pillar will have more “effective” roughness. This acts as a stress concentration points/planes which will deform the pillars at a lower stress because this non-uniformity indicates a higher roughness of the pillar wall, which is responsible for creating more surface nucleated dislocations that will speed up the deformation process. Jennening et al [64] mentioned this dislocation source effect, but with different interpretation.

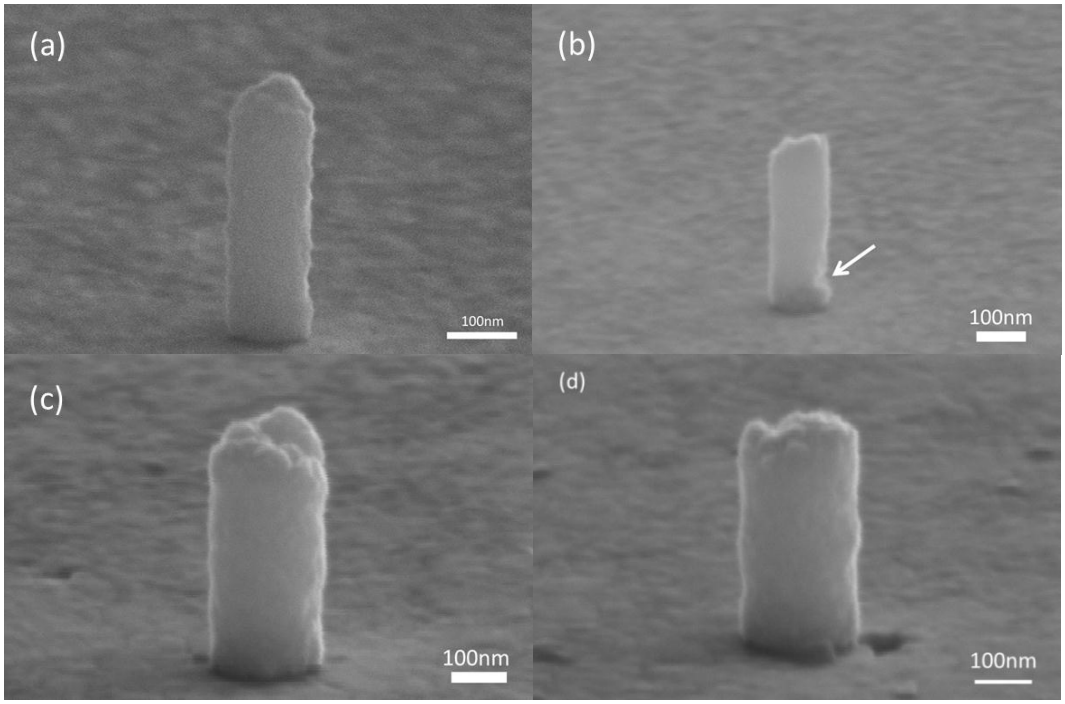

Figure 3.15: The non-uniformity/high roughness of the wall surfaces of 125nm (a & b) and 205 nm (c & d) pillars' diameters.

This problem of high surface roughness for small pillars could be avoided by using FIB techniques to fabricate the pillars. Figure 3.16 shows the difference between the electroplated pillar fabricated in this study and a FIB fabricated pillar of the same size.

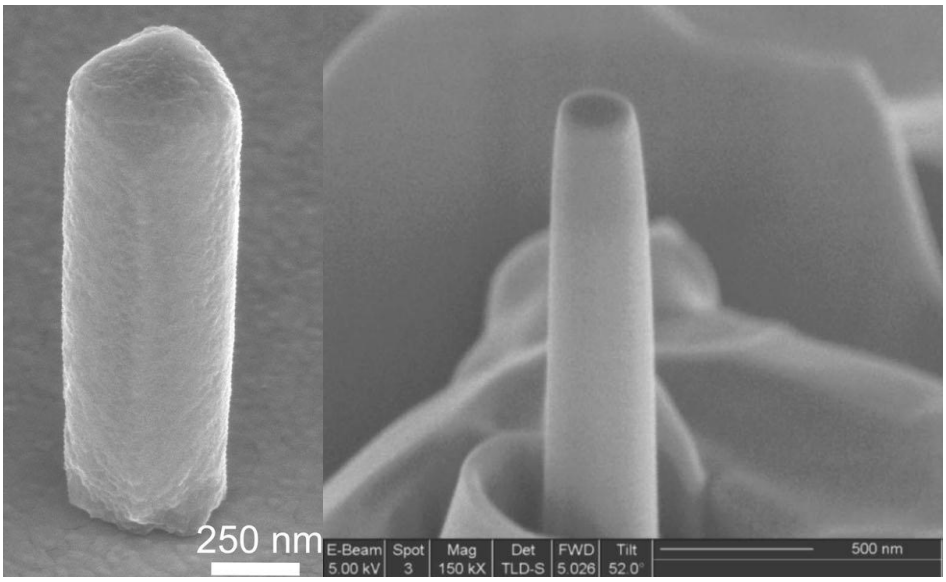

Figure 3.16: Two pillars with almost the same diameter. The left pillar was made of Cu fabricated by electroplating [54] while the left one is Au pillar fabricated by FIB [81]. The roughness is clearly much higher in the case of the electroplated pillar. Reproduced with permissions from [54] and [81].

Another problem that causes the small sized pillars –this is only for the 205nm sample- to be excluded from the increasing trend is the adhesion layer thickness compared to the pillars height. The adhesion layer thickness is 120nm (20 for Ti and 100 for Au) and the pillars heights are close to the adhesion layer thickness (in average, the height is 550 nm for the 205nm diameter pillars). An analogy can be made to demonstrate such problem: if you have a 15cm thick clay bar that is on top of a table, and you want to break a pencil on top of it. If the pencil's height is 30cm, half of the pencil will sink into the clay bar without being deformed. Similarly, if we want to have sufficient strain (30% or more) in addition to the adhesion layer thickness, the pillar will sink until the indenter tip will reach the outer-most free gold layer before the pillar reaches the Si substrate and get compressed consequently. This will add up an 8x8 μm^2 of gold, the tip area, to the stress calculations. Such effect is clearly demonstrated in Figure 3.17.

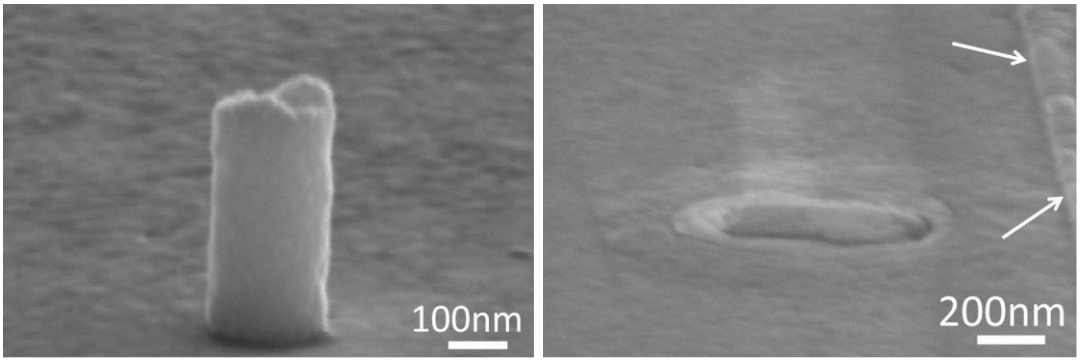

Figure 3.17: Pre- and post-compression images for a 205nm diameter pillar. Note that the pillar completely sank into the adhesion layer and the indenter compressed the free Au surface that is surrounding the pillar as indicated by the arrows.

Another solution might be to increase the aspect ratio, i.e. the pillars height, but this is not appropriate because it will introduce the problem of buckling that was discussed earlier. Another possible solution is to fabricate a substrate with an adhesion layer made from a metal that is harder than Rh and less hard than Si. The problem with this solution is that all active metals are softer than Rh. The solution might be using a composite that is conductive but is harder than Rh.

This problem was not seen in 125nm pillars because they become weaker than Au and Ti -as discussed earlier- so they will not sink in the adhesion and conduction layers. An evidence for this is the deformation of the 125nm pillars (even buckling) without sinking in the adhesion layer, as shown in Figure 3.12 and Figure 3.18.

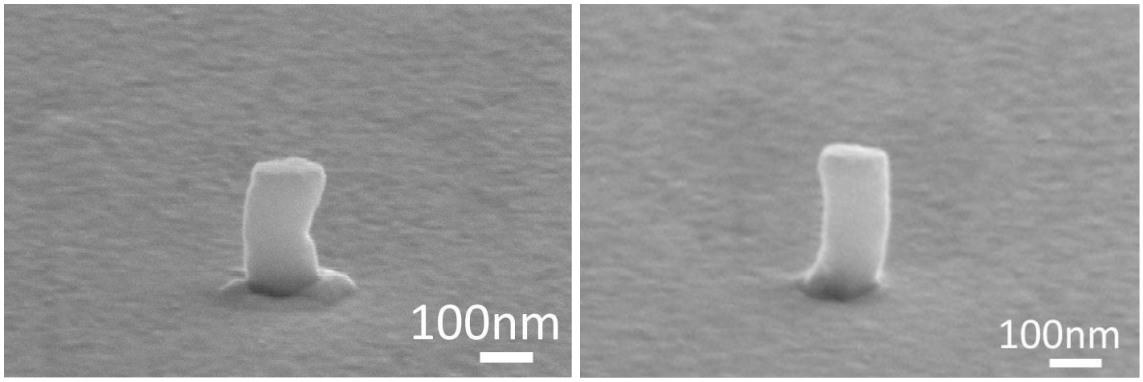

Figure 3.18: 125nm Rh pillars deformed plastically on top of Au. Rhodium nanopillars become weaker/softer than gold at this size.

3- The last scenario is based on the assumption that the 535nm samples had an experimental problem. This will lead to excluding the 535nm sample from the calculations. Such exclusion will lead to the yield stress falling perfectly linearly from 1135 to 125nm through the 205nm diameter pillars. Consequently, the third scenario is a combination of the two previous interpretations/scenarios: the size effect occurs with an increase in the yield point until 1135nm (or maybe at X_n where $1135 \geq X_n \geq 535$ nm) and then falls linearly after that. This may be evidenced by the perfectly linear curve for the 125, 205, and 1135nm diameters samples commensurate with other findings for other metals.

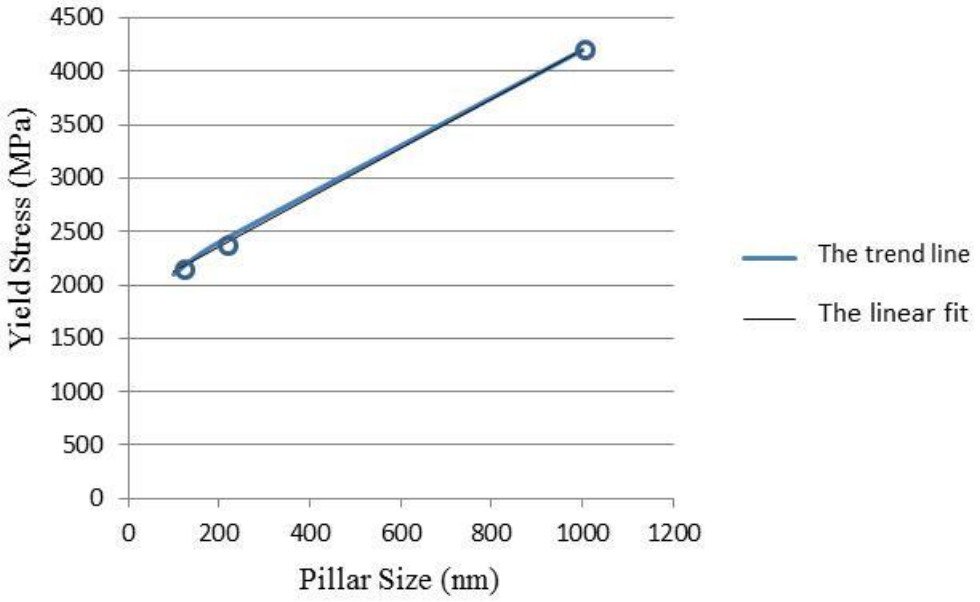

Figure 3.19: The linear relation between the size and the strength of pillars excluding the 535nm sample. The blue line is the real line where the black one is the linear fit for it.

As for choosing the best scenario, the second scenario appears to be the best as it allows for further investigation that will give more certain conclusions.

4. Conclusion and Future Work

The mechanical behaviour of rhodium was shown here and compared with the bulk rhodium behaviour to show the size reduction effect on rhodium mechanical behaviour. The size reduction effect shown here was not the same for all sizes: reduction of the size from the bulk down to the 1135-535 nm range showed a huge increase in the yield point from 67 MPa to 4400 MPa. After that further reduction of the size (i.e. diameter) inverse the effect; meaning, the yield point reduced with the reduction of size. Such transition from strengthening to weakening was attributed to the nanocrystallinity of the fabricated pillars where two basic deformation modes were acting simultaneously: grain boundary-mediated mode and dislocation-driven mode. Beyond about 535nm diameter, the grain boundary-mediated mode predominates over the dislocation-driven one; hence, weakens the material. However, strengthening to weakening transition might also be attributed to extrinsic reasons related to the instrument or to the fabrication process showed in the study for the small sized pillars. To have precise judgment whether the transition is due to intrinsic or extrinsic, further investigation of Rh nanopillars mechanical properties should be done. These investigations should meet the following conditions/criteria:

1- Using FIB or electroplating but at the highest possible plating temperature (50 °C in the solution used here) to insure having pillar walls that are highly smooth to avoid the variation in the data of small sized pillars.
2- Including more variables. For example, recent studies by Jennings et al [64] and Tsui et al [30] showed that copper and tin nanopillars showed a strain rate dependence. As reported above, Rh is independent of strain rate, but this might not hold at the nanoscale. Therefore, it is recommended to confirm the conclusion of

Jennings et al [64], and to see if it can be generalized (i.e. increasing rate dependence with decreasing diameter) and be applicable for metals like rhodium.

3- Narrowing the diameter range under investigation to be from 500nm downward. This is because the transition from dislocation-driven deformation to grain sliding (from smaller-is-stronger to smaller-is-weaker; in other words, the failure of plasticity theory) happened after 500nm but the precise transition-diameter –that is less than or equal 500nm- could not be identified experimentally because of the aforementioned difficulties.

Further studies are recommended into other properties of Rh nanopillars (i.e. electrical, magnetic, etc.) to compliment current report about Rh nanomechanics in order to understand their feasibility in practical applications.

As bulk iridium and ruthenium have almost equivalent strengths to rhodium [39], it is suggested to study the nanomechanical properties of iridium and ruthenium, and compare the results to that of this study, to identify correspondence/match between Ir, Ru, and Rh at the nanoscale in relation to the correspondence/match in their bulk forms. Moreover, another such comparison might be conducted between rhodium, tungsten, and molybdenum (in addition to iridium, and ruthenium) as they share the same bulk strength, but on the homologous temperature scale.

Appendices

The following is a manual for using the following nanoindenter: NanoIndenter® G200, Agilent Technologies Inc. I wrote it for the students in our lab. Other students in other labs operating the same indenter may benefit from it after making some alterations to account for differences between the setups.

For first time users, go to "NanoHand set" → Right click → Click on "Initialization" → wait until the stage stops.

1- Slide the chip into the sample holder. Make sure that the top of the sample's holder is in the same plane as the surface of the chip. (The chip's surface being a little bit higher that the sample holder is better than being little bit lower.) **Make sure that the orientation of the array that you see with unaided eye is opposite, upside down, to what you saw in SEM. (Eventually, the orientation will turn to be as in SEM under the optical microscope).**
2- Slide the sample holder into the stage (beneath the microscope).
3- Open the program that operates the machine *NanoSuite.*
4- Click on "Method" drop down menu → "Open Method" → "Advanced" → Choose "Lee" → Double click on "LEECompressionTest_ConstDisp……."
5- Right click onto the corresponding position of the sample (usually the bottom right circle) → Choose "Move to Target". This will bring the microscope to the top of the sample (chip).
6- Right click and choose "Nano video Handset".
7- Manually, turn on the microscope's light.

8- Now you will see the sample on the screen. Adjust the focus by clicking on the arrows (up or down). Be aware that by clicking the bold arrows you will move the microscope fast which might lead to hitting the chip and destroying it or scratching the microscope's lens. **Moreover, raising the microscope lens too much may turn all arrows (buttons) into position where they turn into lowering the microscope (turning all arrows, whether up or down, into up lifting).**

9- Once you get the right focus, move the microscope around by left clicking on the direction where you want the microscope to move to. Move it around until you see the pillars (they will appear as dots.) Note: It is highly recommended to write down the (x,y) position of the pillars before moving to the next step in order to return to the previous pillars easily.

10- The previous step is to check whether one gets the right orientation of the pillars (as appeared under SEM).

11- Now, move the microscope towards the indium tab. (You must know where is the indium tab relative to the array). **After moving the microscope to a new location and before doing any action you MUST right click and choose "Remove Backlash" to readjust the location of the microscope (and the indenter tip simultaneously) to the true one.**

12- You will know that you are on top of the indium tab by seeing the screen turn black. Upon seeing the screen black, refocus the picture as described in step number 8.

13- Right click and choose “Microscope to Indenter Calibration” → 40X → Click “Advanced Setting”.

14- Change the following:

Number of Indents	1
Distance from Center	25
Depth into Surface	3000

When the “Number of Indents” equals “1” the second factor “Distance from Center” becomes meaningless, but when >1, it becomes important because if you have more than one indent you will have a center that you want to adjust while if you have only one indent, there will be no center to have a value for its distance.

15- Click on “Next”→ “Remove backlash” →click on “Next” → wait until the indent(s) gets done.

16- After finishing indenting the indium tab, if you see the center of the pointer (the red cross) coincides with the center of the indent, click “Finish”. If the centers do not coincide, left click on the center of the indent and then click on “Remove backlash”. Repeat the process until the pointer’s center coincides with the square indent center.

17- Create an Excel test log file. (Describing how to create a test log is out of this manual’s purpose though it is easy).

18- Go back to the “Nano Video Handset” screen (you find such button when right clicking).

19- Move the microscope back to the array and refocus.

20- Click on Batch Mode button (its symbol contains triple III Roman numerals with one of them inside an open file).

21- Click on “Define” (at the left edge of the screen as one of three tabs) → “Next Step” → Unclick the three squares on the right hand side which begins with *Print…., Review Sample….., Review Test….* Respectively →“Next Step” → “Next Step” → Type the file name as the following example: Rh_500nm_Chip611_2nms_3x1_9pillars”.

Note: The 2nms is the displacement rate which should be 2nm/s but the file name does not accept dashes.

22- Click “Next Step” → and change “Delta x” and “Delta y” and the “Drift rate”. “Delta x” and “Delta y” are the (x,y) coordination of the position in microns relative to the (0,0) point which will be the position of the first pillar to be compressed. This position will be the one where the tip will move down to approach the surface of the chip in order to know the position of the surface relative to the pillars tip. The following example will clarify how to choose to choose “Delta x” and “Delta y”.

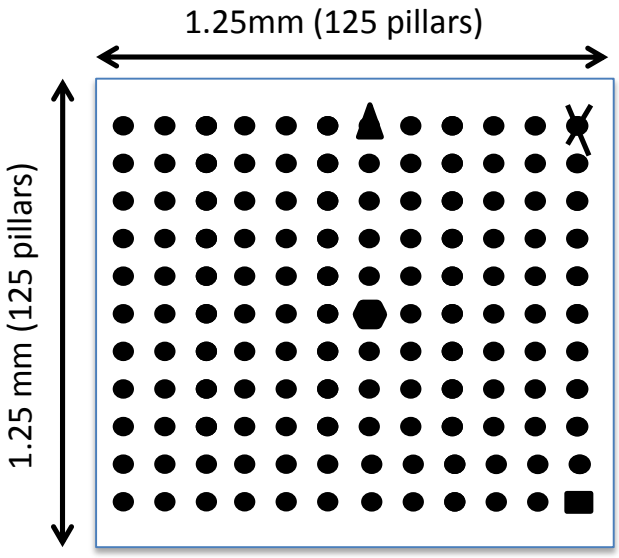

If the crossed pillar is the first to be compressed, “Delta x” is ≥ 10 and “Delta y”

will be ≥ 10. *Note: 10 is an arbitrary number chosen to make the surface approach reasonably far from the array.*

If the square pillar is the first to be compressed, "Delta x" is approximately ≥ 10 and "Delta y" will be ≥ -10 (negative 10).

If the triangular pillar is the first to be compressed, "Delta x" will be =0 "Delta y" will be ≥ 10.

If the hexagonal pillar is the first to be compressed, "Delta x" will be ≥ 75 "Delta y" will be ≥ 75. Note that "Delta x" and "Delta y" could be both ≥ -75.

As for the drift rate, it is the allowable amplitudes for the tip to vibrate with in. So, it should be much smaller than the displacement rate. For example, a 1nm/sec displacement rate should have at most 0.01 drift rate. In mathematical notation, the drift rate in such case could be written as 1±0.01 nm/sec.

23- Click on "Next Step" → and only change the "Surface approach distance". Recall that in step 22 we have to define "Delta x" and "Delta y" so that the tip could find a plane where there is no pillars in order to find –feel- where is the surface of chip. After doing so the tip will move up again to a distance before start compressing. The height that the tip will go to after touching the surface of the chip is the "Surface approach distance". Therefore, the height should be higher than the pillars that will be compressed. For example, if the array pillars are 1000 nm in height, the "Surface approach distance" should be greater than 1000nm. As a safety factor, make the "Surface approach distance" according to the following equation

Surface approach distance= 3 x Pillar Height (in nanometers)

Note: Be aware that some variables are defined in microns while others are defined in nanometers.

24- Click on "Next Step" → and change two variables: "Prescribed Displacement Rate" and "Prescribed Length Change". The "Prescribed Displacement Rate" is clear. The "Prescribed Length Change" is how far the indenter tip compresses from the top surface of the pillar. It is recommended for some experiments that this length change be 30% of the pillar height. For example, if you have 1000nm high pillars, the "Prescribed Length Change" will be 300nm.

25- Click on "Next Step" → and click on first pillar you want to compress → click on "Remove backlash" → click on "Add Test to this Location". Repeat this process for the rest of the pillars you want to compress.

26- Click on "Next Step" → and click on "No".

27- Go back to the test view by clicking on "Test" tab on the left hand side of the screen.

28- Click on the green rectangular to let the test begin.

29- Turn off the microscope light.

The five NEVER DO actions:

1- Raising the microscope too much when focusing the image.

2- Moving the microscope two times without removing the backlash.

3- Adding higher number to the “Prescribed Length Change” by mistake. For example, instead of typing 300 you write 3000! This will destroy the tip as it will indent the whole chip and move to indent the Indenter base or stage.

4- Sliding the chip into the chip holder while the chip surface is below the surface of the edges of the chip holder.

5- Not moving the microscope up before removing the sample.

Permissions

AMERICAN PHYSICAL SOCIETY
One Physics Ellipse, College Park, MD 20740 · http://www.aps.org

October 27, 2011

Omar Dhafer Ali Alshehri
University of Waterloo

Ref # 10716

Thank you for your permission request dated October 19, 2011. We are pleased to grant you a non-exclusive, non-transferable permission, English rights, limited to **print and World Wide Web format only**, provided you meet the criteria outlined below. Permission is for a one-time use and does not include permission for future editions, updates, additional electronic forms, databases, translations, or any other matters. Permission must be sought for each additional use. This permission does not include the right to modify APS material.

Please print the required copyright credit line on the first page that the material appears: "Reprinted (abstract/excerpt/figure) with permission from [FULL REFERENCE CITATION] as follows: authors names, journal title, volume number, page number and year of publication. Copyright (YEAR) by the American Physical Society.

The following language must appear somewhere on the website: "Readers may view, browse, and/or download material for temporary copying purposes only, provided these uses are for noncommercial personal purposes. Except as provided by law, this material may not be further reproduced, distributed, transmitted, modified, adapted, performed, displayed, published, or sold in whole or part, without prior written permission from the American Physical Society."

Provide a hyperlink from the reprinted APS material (the hyperlink may be embedded in the copyright credit line). APS's link manager technology makes it convenient and easy to provide links to individual articles in APS journals. For information, see: http://link.aps.org/.

You must also obtain permission from at least one of the authors for each separate work, if you haven't done so already. The author's name and address can be found on the first page of the published Article.

Use of the APS material must not imply any endorsement by the American Physical Society.

Permission is granted for use of the following APS material only:

- Fig. 1, Phys. Rev. B 73, 245410 (2006)

Permission is limited to the single title specified or single edition of the publication as follows:

- Thesis by Omar Dhafer Ali Alshehri to be published by the University of Waterloo

If you have any questions, please refer to the Copyright FAQ at: http://publish.aps.org/copyrightFAQ.html or send an email to assocpub@aps.org.

Sincerely,

[redacted]

Eileen LaManca
Publications Marketing Coordinator

ELSEVIER LICENSE

This is a License Agreement between Omar D Alshehri ("You") and Elsevier ("Elsevier") provided by Copyright Clearance Center ("CCC"). The license consists of your order details, the terms and conditions provided by Elsevier, and the payment terms and conditions.

The licence number: 2771980710386.

The licence date: Oct 18, 2011.

Licensed content title: Emergence of strain-rate sensitivity in Cu nanopillars: Transition from dislocation multiplication to dislocation nucleation.

Licensed content publication: Acta Materialia.

Licensed content author: Andrew T. Jennings,Ju Li,Julia R. Greer.

Note: I contacted Elsevier for providing a formal signed letter but they refused.

RSC Publishing

Royal Society of Chemistry
Thomas Graham House
Science Park
Milton Road
Cambridge
CB4 0WF

Tel: +44 (0)1223 420 066
Fax: +44 (0)1223 423 623
Email: contracts-copyright@rsc.org

www.rsc.org

PUBLISHING SERVICES

Omar Alshehri
G505- 196 Westmount Rd N
Waterloo, ON
N2L 3G5
Canada

12th December 2011

Dear Dr Alshehri

The Royal Society of Chemistry hereby grants permission for the use of the material specified below in the work described and in all subsequent editions of the work for distribution throughout the world, in all media including electronic and microfilm. You may use the material in conjunction with computer-based electronic and information retrieval systems, grant permissions for photocopying, reproductions and reprints, translate the material and to publish the translation, and authorize document delivery and abstracting and indexing services. The Royal Society of Chemistry is a signatory to the STM Guidelines on Permissions (available on request).

Please note that if the material specified below or any part of it appears with credit or acknowledgement to a third party then you must also secure permission from that third party before reproducing that material.

Please ensure that the published article carries a credit to The Royal Society of Chemistry in the following format:

[Original citation] – Reproduced by permission of The Royal Society of Chemistry

and that any electronic version of the work includes a hyperlink to the book on the Royal Society of Chemistry website at http://www.rsc.org/Shop/books/2008/9781847558954.asp.

Yours sincerely

[redacted]

Gill Cockhead
Publishing Contracts & Copyright Executive

The material being reproduced is as follows:

Book Title:	*Nanochemistry: a Chemical Approach to Nanomaterials 2nd Edition*
Authors:	Geoffrey A. Ozin and André C. Arsenault, Ludovico Cademartiri
Year of Publication:	2009
Material:	Two cartoons on pages XVIII-XIX

and it is going to be reproduced in the following publication:

Thesis Title:	*Mechanical Behaviour of Nanocrystalline Rhodium Nanopillars under Compression*
Author:	Omar Dhafer Alshehri
Publisher:	University of Waterloo, Canada

VAT Registration Number: GB 342 1764 71

Registered Charity Number: 207890

INTERNATIONAL
Standards Worldwide

Address 100 Barr Harbor Drive
PO Box C700
W. Conshohocken, PA
19428-2959 | USA

Phone 610.832.9500
Fax 610.832.9555
e-mail service@astm.org
Web www.astm.org

12 January 2012

Dear Omar:

In response to your email today, ASTM International grants a limited non-exclusive license to reproduce Table V from the article Tensile Properties of the Platinum-Group Metals, in your thesis titled, "Mechanical Behaviour of Nanocrystalline Rhodium Nanopillars," provided the following credit line is used:

> "Reprinted, with permission, from ASTM STP 272 Symposium on Newer Metals, copyright ASTM International, 100 Barr Harbor Drive, West Conshohocken, PA 19428."

Thank you for your interest in ASTM publications.

Kind regards,

[redacted]

Kathe Hooper
Manager, Rights and Permissions

kh

Bibliography

[1] nobelprize.org, "Nobel Prize Interview with Heinrich Rohrer," ed, 2008.

[2] L. S. Jeffrey, *American inventors of the 20th century*: Enslow Publishers, 1996.

[3] R. M. Barnes, *Motion and time study: design and measurement of work*: Wiley, 1980.

[4] J. Al-Khalili. (2009, 09/11/2011). The 'first true scientist'. Available: http://news.bbc.co.uk/2/hi/7810846.stm

[5] D. Ellyard, *Who Discovered What When*: New Holland, 2006.

[6] Alhazen and A. I. Sabra, *The Optics of Ibn al-Haytham. Books I-III, On direct vision*. London: Warburg Institute, University of London, 1989.

[7] Alhazen and A. M. Smith, *Alhacen's theory of visual perception: a critical edition, with English translation and commentary, of the first three books of Alhacen's De aspectibus, the medieval Latin version of Ibn al-Haytham's Kitab al-Manazir*. Philadelphia: American Philosophical Society, 2001.

[8] S. Drake, T. H. Levere, and W. R. Shea, *Nature, experiment, and the sciences: essays on Galileo and the history of science* vol. 120: Springer, 1990.

[9] "Hans Jansen," in *Encyclopedia Britannica*, On-line Academic ed, 2011.

[10] R. P. Feynman, "There's plenty of room at the bottom," *Engineering and Science*, vol. 23, pp. 22-36, 1960.

[11] G. Binnig and H. Rohrer, "Scanning tunneling microscopy," *Surf. Sci.*, vol. 126, pp. 236-244, 1983.

[12] E. Ruska, "The early development of electron lenses and electron microscopy," *Microscopica acta. Supplement*, p. 1, 1980.

[13] A. H. Zewail, "Laser femtochemistry," *Sci*, vol. 242, p. 1645, 1988.

[14] R. Piquepaille, "The world's fastest camera."

[15] A. H. Zewail, "4D ultrafast electron diffraction, crystallography, and microscopy," *Annu. Rev. Phys. Chem.*, vol. 57, pp. 65-103, 2006.

[16] nobelprize.org, "Nobel Prize Interview with Alexei A. Abrikosov," ed, 2003.

[17] C. Burda, X. Chen, R. Narayanan, and M. A. El-Sayed, "Chemistry and Properties of Nanocrystals of Different Shapes," *Chem. Rev.*, vol. 105, pp. 1025-1102, 2005/04/01 2005.

[18] M. Zhang, K. R. Atkinson, and R. H. Baughman, "Multifunctional Carbon Nanotube Yarns by Downsizing an Ancient Technology," *Sci*, vol. 306, pp. 1358-1361, November 19, 2004 2004.

[19] A. K. Geim and K. S. Novoselov, "The rise of graphene," *Nature materials*, vol. 6, pp. 183-191, 2007.

[20] G. A. Ozin and A. C. Arsenault, *Nanochemistry: a chemical approach to nanomaterials*: Royal Society of Chemistry, 2005.

[21] Munir Nayfeh, Zain Yamani, and a. H. Nayfeh, "Nanotechnology and the 21st Century," in *ALECSO* vol. 3, ed. Tunisia: Arab League, 1998.

[22] B. Rogers, J. Adams, and S. Pennathur, *Nanotechnology: understanding small systems*: CRC Press, 2008.

[23] J. V. Barth, G. Costantini, and K. Kern, "Engineering atomic and molecular nanostructures at surfaces," 2006.

[24] M. Uchic, D. Dimiduk, J. Florando, and W. Nix, "Sample dimensions influence strength and crystal plasticity," *Sci,* vol. 305, p. 986, 2004.
[25] A. C. Fischer-Cripps, *Nanoindentation*: Springer Verlag, 2011.
[26] A. T. Jennings and J. R. Greer, "Tensile deformation of electroplated copper nanopillars," *PMag,* vol. 91, pp. 1108-1120, 2011.
[27] S. Barakat, P. Lee-Sullivan, S. A. Vitale, and T. Y. Tsui, "The effects of low temperature and pressure on the fracture behaviors of organosilicate thin films," *J. Mater. Res.,* vol. 26, pp. 2524 - 2532, 2011.
[28] Y. Xiang, X. Chen, and J. Vlassak, "Plane-strain bulge test for thin films," *J. Mater. Res.,* vol. 20, pp. 2360-2370, 2005.
[29] T. Y. Tsui, A. J. McKerrow, and J. J. Vlassak, "Constraint effects on thin film channel cracking behavior," *J. Mater. Res.,* vol. 20, pp. 2266-2273, 2005.
[30] M. J. Burek, A. S. Budiman, Z. Jahed, N. Tamura, M. Kunz, S. Jin, S. M. J. Han, G. Lee, C. Zamecnik, and T. Y. Tsui, "Fabrication, microstructure, and mechanical properties of tin nanostructures," *Materials Science and Engineering: A,* 2011.
[31] M. J. Burek and J. R. Greer, "Fabrication and microstructure control of nanoscale mechanical testing specimens via electron beam lithography and electroplating," *Nano Lett.,* vol. 10, pp. 69-76, 2009.
[32] J. R. Greer, W. C. Oliver, and W. D. Nix, "Size dependence of mechanical properties of gold at the micron scale in the absence of strain gradients," *Acta Mater.,* vol. 53, pp. 1821-1830, 2005.
[33] M. Arbib, B. Zhang, V. Lazarov, D. Stoychev, A. Milchev, and C. Buess-Herman, "Electrochemical nucleation and growth of rhodium on gold substrates," *J. Electroanal. Chem.,* vol. 510, pp. 67-77, 2001.
[34] D. R. Lide, *CRC handbook of chemistry and physics: a ready-reference book of chemical and physical data*: CRC Pr I Llc, 2004.
[35] A. Darling, "Some Properties and Applications of the Platinum-Group Metals," *International Metallurgical Reviews,* vol. 18, pp. 91-122, 1973.
[36] T. Hüpf, C. Cagran, B. Wilthan, and G. Pottlacher, "Thermophysical properties of rhodium obtained by fast pulse-heating," *J. Phys.: Condens. Matter,* vol. 21, p. 125701, 2009.
[37] Z. Szucs, D. Moolman, S. Verryn, and J. R. Zeevaart, "The metal Rhodium does not have allotropes," *J. Radioanal. Nucl. Chem.,* vol. 284, pp. 239-243, 2010.
[38] J. W. Arblaster, "The Discoverers of the Rhodium Isotopes," *Platinum Met. Rev.,* vol. 55, pp. 124-134, 2011.
[39] F. Holden, R. Douglass, and R. Jaffee, "Tensile Properties of the Platinum Group Metals," in *Symposium on newer metals,* San Francisco, 1960, pp. 68-79.
[40] R. C. Weast, *CRC handbook of chemistry and physics: a ready-reference book of chemical and physical data*: CRC Press, 1977.
[41] J. Tuoriniemi and T. Knuuttila, "Nuclear cooling and spin properties of rhodium down to picokelvin temperatures," *Physica B: Condensed Matter,* vol. 280, pp. 474-478, 2000.
[42] J. M. Thomas and W. J. Thomas, *Principles and practice of heterogeneous catalysis*: Wiley-VCH, 1997.
[43] G. C. Bond, *Heterogeneous catalysis*: Oxford University Press, New York, 1987.

[44] M. Passoni, D. Dellasega, G. Grosso, C. Conti, M. Ubaldi, and C. Bottani, "Nanostructured rhodium films produced by pulsed laser deposition for nuclear fusion applications," *J. Nucl. Mater.,* vol. 404, pp. 1-5, 2010.
[45] G. Hass, "Reflectance and preparation of front-surface mirrors for use at various angles of incidence from the ultraviolet to the far infrared," *JOSA,* vol. 72, pp. 27-39, 1982.
[46] G. Hu, Z. Zhou, Y. Guo, H. Hou, and S. Shao, "Electrospun rhodium nanoparticle-loaded carbon nanofibers for highly selective amperometric sensing of hydrazine," *Electrochem. Commun.,* vol. 12, pp. 422-426, 2010.
[47] A. Etspüler and H. Suhr, "Deposition of thin rhodium films by plasma-enhanced chemical vapor deposition," *ApPhA,* vol. 48, pp. 373-375, 1989.
[48] S. Petersson, R. Anderson, J. Baglin, J. Dempsey, W. Hammer, F. dHeurle, and S. LaPlaca, "The thin film formation of rhodium silicides," *J. Appl. Phys.,* vol. 51, pp. 373-382, 1980.
[49] E. B. Graper, "Evaporation characteristics of materials from an electron beam gun II," *Journal of Vacuum Science & Technology A: Vacuum, Surfaces, and Films,* vol. 5, pp. 2718-2723, 1987.
[50] A. Perry and N. Archer, "Techniques of Chemical Vapour Deposition," *AGARD, NATO,* vol. 106, p. 16, 1980.
[51] L. Marot, G. De Temmerman, P. Oelhafen, G. Covarel, and A. Litnovsky, "Rhodium coated mirrors deposited by magnetron sputtering for fusion applications," *Rev. Sci. Instrum.,* vol. 78, p. 103507, 2007.
[52] L. Marot, G. Covarel, M. H. Tuilier, R. Steiner, and P. Oelhafen, "Adhesion of rhodium films on metallic substrates," *Thin Solid Films,* vol. 516, pp. 7604-7608, 2008.
[53] F. Orsitto, D. Del Bugaro, M. DiFino, A. Maiolo, M. Montecchi, E. Nichelatti, C. Gowers, and P. Nielsen, "Optical characterization of plasma facing mirrors for a Thomson scattering system of a burning plasma experiment," *Rev. Sci. Instrum.,* vol. 72, pp. 540-544, 2001.
[54] A. T. Jennings, M. J. Burek, and J. R. Greer, "Microstructure versus Size: Mechanical Properties of Electroplated Single Crystalline Cu Nanopillars," *Phys. Rev. Lett.,* vol. 104, p. 135503, 2010.
[55] E. Bale, "The Structure of Rhodium," *Platinum Met. Rev.,* vol. 2, pp. 61-63, 1958.
[56] U. S. D. o. Commerce, "Melting, Mechanical Working, and some Physical Properties of Rhodium," ed. Washington: Bureau of Standards journal of research, 1928, pp. 1029-1040.
[57] D. Maurer, R. Heichele, N. Lingg, V. Müller, and K. Rieder, "Elastic Properties of Purified Single Crystalline Rhodium," *physica status solidi (a),* vol. 160, pp. 403-411, 1997.
[58] E. Walker, J. Ashkenazi, and M. Dacorogna, "Elastic moduli of rhodium: Correct prediction by a new theoretical method," *PhRvB,* vol. 24, pp. 2254-2256, 1981.
[59] N. E. Dowling, *Mechanical behavior of materials: engineering methods for deformation, fracture and fatigue*: Pearson Prentice Hall, 2007.
[60] G. Lee, J. Y. Kim, A. S. Budiman, N. Tamura, M. Kunz, K. Chen, M. J. Burek, J. R. Greer, and T. Y. Tsui, "Fabrication, structure and mechanical properties of indium nanopillars," *Acta Mater.,* vol. 58, pp. 1361-1368, 2010.

[61] G. Lee, J. Y. Kim, M. J. Burek, J. R. Greer, and T. Y. Tsui, "Plastic deformation of indium nanostructures," *Materials Science and Engineering: A*, 2011.
[62] M. J. Burek, S. Jin, M. C. Leung, Z. Jahed, J. Wu, A. S. Budiman, N. Tamura, M. Kunz, and T. Y. Tsui, "Grain boundary effects on the mechanical properties of bismuth nanostructures," *Acta Mater.*, 2011.
[63] Z. Jahed Motlagh, "Mechanical Behaviour of Single Crystal, Pollycrystalline and Nanocrystalline Metallic Nanopillars Under Compression," Master of Applied Science Experimental, Mechanical and Mechatronics Engineering, University of Waterloo, Waterloo, 2011.
[64] A. T. Jennings, J. Li, and J. R. Greer, "Emergence of strain-rate sensitivity in Cu nanopillars: Transition from dislocation multiplication to dislocation nucleation," *Acta Mater.*, 2011.
[65] M. D. Uchic, P. A. Shade, and D. M. Dimiduk, "Plasticity of micrometer-scale single crystals in compression," *Annual Review of Materials Research*, vol. 39, pp. 361-386, 2009.
[66] J. A. El-Awady, C. Woodward, D. M. Dimiduk, and N. M. Ghoniem, "Effects of focused ion beam induced damage on the plasticity of micropillars," *PhRvB*, vol. 80, p. 104104, 2009.
[67] S. H. Oh, M. Legros, D. Kiener, and G. Dehm, "In situ observation of dislocation nucleation and escape in a submicrometre aluminium single crystal," *Nature materials*, vol. 8, pp. 95-100, 2009.
[68] S. W. Lee, S. M. Han, and W. D. Nix, "Uniaxial compression of fcc Au nanopillars on an MgO substrate: The effects of prestraining and annealing," *Acta Mater.*, vol. 57, pp. 4404-4415, 2009.
[69] T. A. Parthasarathy, S. I. Rao, D. M. Dimiduk, M. D. Uchic, and D. R. Trinkle, "Contribution to size effect of yield strength from the stochastics of dislocation source lengths in finite samples," *Scripta Mater.*, vol. 56, pp. 313-316, 2007.
[70] A. Kunz, S. Pathak, and J. R. Greer, "Size effects in Al nanopillars: Single crystalline vs. bicrystalline," *Acta Mater.*, 2011.
[71] C. Frick, B. Clark, S. Orso, A. Schneider, and E. Arzt, "Size effect on strength and strain hardening of small-scale [1 1 1] nickel compression pillars," *Materials Science and Engineering: A*, vol. 489, pp. 319-329, 2008.
[72] D. Dimiduk, M. Uchic, and T. Parthasarathy, "Size-affected single-slip behavior of pure nickel microcrystals," *Acta Mater.*, vol. 53, pp. 4065-4077, 2005.
[73] D. Jang, C. Cai, and J. R. Greer, "Influence of Homogeneous Interfaces on the Strength of 500 nm Diameter Cu Nanopillars," *Nano Lett.*, 2011.
[74] M. Meyers, A. Mishra, and D. Benson, "Mechanical properties of nanocrystalline materials," *Prog. Mater Sci.*, vol. 51, pp. 427-556, 2006.
[75] D. Jang and J. R. Greer, "Size-induced weakening and grain boundary-assisted deformation in 60nm-grained Ni nano-pillars," *Scripta Mater.*, 2010.
[76] E. Hall, "The deformation and ageing of mild steel: III discussion of results," *Proceedings of the Physical Society. Section B*, vol. 64, p. 747, 1951.
[77] N. Petch, "The cleavage strength of polycrystals," *J. Iron Steel Inst*, vol. 174, pp. 25-28, 1953.

[78] Y. Min, M. Akbulut, K. Kristiansen, Y. Golan, and J. Israelachvili, "The role of interparticle and external forces in nanoparticle assembly," *Nat Mater*, vol. 7, pp. 527-538, 2008.
[79] S. Balibar, *The atom and the apple: Twelve tales from contemporary physics* 1st ed.: Princeton University Press, 2008.
[80] Z. Shan, E. Stach, J. Wiezorek, J. Knapp, D. Follstaedt, and S. Mao, "Grain boundary-mediated plasticity in nanocrystalline nickel," *Sci*, vol. 305, p. 654, 2004.
[81] J. R. Greer and W. D. Nix, "Nanoscale gold pillars strengthened through dislocation starvation," *PhRvB*, vol. 73, p. 245410, 2006.